A pure marine aerosol model, for use in remote sensing applications

A. M. Sayer,[1,2] A. Smirnov,[2,3] N. C. Hsu,[2] B. N. Holben[2]

Abstract. Retrievals of aerosol optical depth (AOD) and related parameters from satellite measurements typically involve prescribed models of aerosol size and composition, and are therefore dependent on how well these models are able to represent the radiative behaviour of real aerosols. This study uses aerosol volume size distributions retrieved from Sun-photometer measurements at 11 Aerosol Robotic Network (AERONET) island sites, spread throughout the world's oceans, as a basis to define such a model for unpolluted maritime aerosol. Size distributions are observed to be bimodal and approximately lognormal, although the coarse mode is skewed with a long tail on the low-radius end. The relationship of AOD and size distribution parameters to meteorological conditions is also examined. As wind speed increases, so do coarse-mode volume and radius. The AOD and Ångström exponent (α) show linear relationships with wind speed, although there is considerable scatter in all these relationships, limiting their predictive power. Links between aerosol properties and near-surface relative humidity, columnar water vapor, and sea surface temperature are also explored. A recommended bimodal maritime model, which is able to reconstruct the AERONET AOD with accuracy of order 0.01-0.02, is presented for use in aerosol remote sensing applications. This accuracy holds at most sites and for wavelengths between 340 nm and 1020 nm. Calculated lidar ratios are also provided, and differ significantly from those currently used in Cloud-Aerosol Lidar with Orthogonal Polarization (CALIOP) processing.

1. Introduction

The size distribution and spectral complex refractive index of aerosols are needed to compute properties such as their scattering phase function, single scatter albedo, and extinction coefficient, which are in turn used to calculate quantities such as total aerosol optical depth (AOD) from column abundance. The information content of measurements from current satellite radiometers is insufficient to unambiguously retrieve all these parameters, particularly when the (spectral and directional) behaviour of surface reflectance is unknown (*Hasekamp and Landgraf*, 2007). For this reason, aerosol retrieval algorithms employed by most of these sensors are required to make assumptions about aerosol microphysical properties and rely on a set of predefined aerosol models or components. The assumptions in these aerosol retrieval algorithms contribute to differences in retrieved AOD, even in the idealised case of a black (non-reflecting) surface (*Kokhanovsky et al.*, 2010). The Polarization and Directionality of the Earth's Reflectance (POLDER) sensor is an exception to this, as its measurement capabilities provide an increased information content as compared to other current sensors (*Dubovik et al.*, 2011, *Hasekamp et al.*, 2011).

For other sensors, it is therefore of high importance that the models used are representative of real aerosol properties. The purpose of this study is to develop such a model for clean maritime aerosol, using Sun-photometer data from the Aerosol Robotic Network (AERONET; *Holben et al.*, 1998). A companion paper, *Sayer et al.* [2011], describes the application of this model to aerosol retrievals from Sea-viewing Wide Field-of-view Sensor (SeaWiFS) measurements.

Datasets including the optical properties of marine aerosol as determined from ground-based measurements, aircraft, remote sensing, or theoretical considerations exist, and a review of some of these is presented by *Smirnov et al.* [2002]. In particular, the models of *Shettle and Fenn* [1979] (from aircraft measurements) and *Gathman* [1983] (coastal towers, and ships) have been used widely. However, observational datasets are typically limited in time and space, and differences between the types of instrumentation used in these campaigns contribute to significant differences between the results (*Reid et al.*, 2006). Advantages of the AERONET data therefore include the opportunity for a longer time series, with a wide global distribution, and consistency between different measurement sites. Such studies are also often coastal, such that there may be a non-maritime component to the aerosol. While still a factor for AERONET data, this can be minimised through choice of remote sites and careful filtering of data. A previous AERONET-based analysis was performed by *Smirnov et al.* [2003a], although at that time the available data record was smaller.

The aerosol number size distribution $dN(r)/d\ln(r)$ describes the number of aerosol particles with radius in the infinitesimal size range $r \pm d\ln(r)$. The distribution is also sometimes defined as $dN(r)/d\,r$, and these two are easily related by

$$\frac{dN(r)}{dr} = \frac{d\ln(r)}{dr}\frac{dN(r)}{d\ln(r)} = \frac{1}{r}\frac{dN(r)}{d\ln(r)}. \quad (1)$$

The volume size distribution, calculable for spherical aerosol particles as

$$\frac{dV(r)}{d\ln(r)} = \frac{4\pi r^3}{3}\frac{dN(r)}{d\ln(r)}, \quad (2)$$

[1]Goddard Earth Sciences Technology and Research (GESTAR), Universities Space Research Association.

[2]NASA Goddard Space Flight Center, Greenbelt, MD, USA.

[3]Sigma Space Corporation, Lanham, MD, USA.

0148-0227/11/$9.00

describing the aerosol particle volume over the same infinitesimal radius range, is also frequently used. The AERONET products are defined in terms of the columnar volume size distribution and so this convention is adopted in the analysis here. The total aerosol columnar particle number (C_n) and volume (C_v) are obtained by integrating these distributions over all $\ln(r)$.

Frequently-used metrics to characterise aerosol size distributions include the volume mean radius (r_v) as a measure of the size of the aerosol particles, where

$$\ln(r_v) = \frac{\int_{-\infty}^{\infty} \ln(r) \frac{dV(r)}{d\ln(r)} d\ln(r)}{\int_{-\infty}^{\infty} \frac{dV(r)}{d\ln(r)} d\ln(r)}, \quad (3)$$

and the standard deviation (or spread) of the distribution (σ) as a measure of the dispersion:

$$\sigma = \sqrt{\frac{\int_{-\infty}^{\infty} (\ln(r) - \ln(r_v))^2 \frac{dV(r)}{d\ln(r)} d\ln(r)}{\int_{-\infty}^{\infty} \frac{dV(r)}{d\ln(r)} d\ln(r)}} \quad (4)$$

In the above the integration is theoretically carried out over all $\ln(r)$, although in practical applications some minimum and maximum bounds on the radius are defined as cutoffs, outside which the aerosol number and volume are negligible. The mean radius of the number distribution r_n is defined analagously to Equation 3, using $dN(r)/d\ln(r)$ in place of $dV(r)/d\ln(r)$. A third useful quantity is the effective radius (r_{eff}), the ratio of the third to second moments of the number size distribution:

$$r_{eff} = \frac{\int_{-\infty}^{\infty} r^3 \frac{dN(r)}{d\ln(r)} d\ln(r)}{\int_{-\infty}^{\infty} r^2 \frac{dN(r)}{d\ln(r)} d\ln(r)}, \quad (5)$$

The effective radius is more closely related to aerosol extinction than the number median radius because scattering depends on aerosol cross-sectional area, and distributions with similar effective radii (and effective variances, although this quantity is not frequently used in aerosol studies) typically have similar scattering properties, even if the precise modal radii and spreads differ (*Hansen and Travis*, 1974, *Mishchenko et al.*, 1997).

Aerosol size distributions are commonly represented as a combination of lognormally-distributed components, in which case the number size distribution is defined as a summation over these (n_c) components by

$$\frac{dN(r)}{d\ln(r)} = \sum_{i=1}^{n_c} \frac{C_{n,i}}{\sqrt{2\pi}\sigma_i} e^{-\frac{1}{2}\left(\frac{\ln(r) - \ln(r_{n,i})}{\sigma_i}\right)^2}, \quad (6)$$

and the modal radius for each component is also its median and geometric mean. The equivalent distribution for aerosol volume is arrived at by substituting r_n with r_v, and C_n with C_v. The advantages of lognormal distributions include that their statistical properties are well-known, and many available radiative transfer codes are able to take as input lognormal distribution parameters. For individual lognormal components, the conversion between the volume and number distribution parameters is presented in Appendix A. Note that the spread σ remains the same for both number and volume distributions. *Hinds* [1999] presents some general results for moments of lognormal distributions, including that

$$r_{eff} = r_n e^{2.5\sigma^2} = r_v e^{-0.5\sigma^2}. \quad (7)$$

Section 2 describes the AERONET data used, and properties of average size distributions. Section 3 examines the effect of meteorology on the size distribution. Next, Section 4 combines the size information with various refractive indices to define an average aerosol model which is best able to replicate the observed AERONET AODs. Following the definition of this model, Section 5 tests the predictive power of relationships observed between wind speed and aerosol volume on ship-borne AOD measurements, and Section 6 presents calculated lidar ratios. Finally, Section 7 summarises the results of the study.

2. AERONET sites and size distribution data

2.1. Sites and data selection criteria

AERONET data from sites listed in Table 1, and shown in Figure 1, are used here to investigate the characteristics of maritime aerosol. These sites have been chosen due to their general remoteness from local sources, to maximise the chances of measuring unpolluted maritime aerosol, and span a variety of oceans. The stability and pointing accuracy required to perform the almucantar scans used to retrieve the size distribution means they are impractical to perform aboard moving platforms such as ships, and so island sites represent the closest to open-ocean conditions which can be obtained using this technique. Of these sites Lanai, Bermuda, and Kaashidhoo were previously studied by *Smirnov et al.* [2003a]. A similar study, also examining the effect of wind speed on aerosol properties, was performed for Midway Island by *Smirnov et al.* [2003b]. The main development of this study over previous work is the improved data record, in terms of an increased number of observations over a larger number of locations, and taking advantage of more recent AERONET algorithm improvements (*Holben et al.*, 2006). Additionally, some meteorological aspects, and refractive index, are examined in more detail. *Ahmad et al.* [2010] also used AERONET inversions to inform aerosol models for satellite retrieval, but with a different approach, and did not filter for 'pure maritime' cases in this way.

For all sites except Graciosa, only version 2 level 2.0 (cloud-screened and quality-assured; *Smirnov et al.*, 2000a, *Holben et al.*, 2006) data are ised. Only retrievals from 1999 onwards are considered as the newer Sun photometers deployed since then enable a higher data quality. Graciosa is a comparatively new AERONET site (established in 2009) and some of the earlier measurements are suspected of cloud-contamination problems; only level 1.5 (cloud-screened) data collected in 2010 are used here as they are thought to be largely free of this, although have not yet been formally raised to level 2.0. Graciosa is used in preference to the nearby Azores site (which does have level 2.0 data) as the former is in a more remote setting and has a larger data record. Despite small data records and/or increased chance of influence from other aerosol types, Kaashidhoo, Ascension Island, and Amsterdam Island are included in the analysis as the most suitable (or only) sites in their respective regions. In particular, Kaashidhoo samples air masses transported from the Indian subcontinent, south-east Asia, the Arabian Sea, and the Southern Indian Ocean (*Lobert and Harris*,

2002), while Ascension Island can be affected by transported African biomass burning emissions (*Galanter et al.*, 2000). Crozet Island has a small data record, due primarily to frequent cloud cover, and has the highest elevation above sea level (221 m, so still within the marine boundary layer), but is included nonetheless as, unlike the majority of other sites, it occupies a cool-sea and high-wind environment.

The AERONET inversion algorithm used to retrieve the aerosol size distribution (in 22 logarithmically-spaced size bins) and refractive index from Sun-photometer measurements is described by *Dubovik and King* [2000] and *Dubovik et al.* [2006]. It takes as input diffuse-sky radiances at 440 nm, 675 nm, 870 nm, and 1020 nm in the solar almucantar, as well as AODs and water vapor from direct-Sun measurements averaged for 16 minutes before and after the almucantar scan. As in *Smirnov et al.* [2003a], in this study the level 2.0 AERONET inversions are filtered to select only those retrievals which likely correspond to clean maritime aerosol. These constraints are based upon the measured AOD and retrieved size distribution. Here, τ_λ denotes the AOD at wavelength λ (in nm), and α the Ångström parameter, which describes the spectral variability of τ. From the observations of *Ångström* [1929] that $\tau_\lambda \approx \beta\lambda^{-\alpha}$ (where the turbidity coefficient β is the AOD at 1 μm), typically the definition $\alpha = -d\ln(\tau)/d\ln(\lambda)$ is used, and α calculated between a pair of wavelengths λ_1, λ_2 as

$$\alpha_{\lambda_1,\lambda_2} = -\frac{[\ln(\tau_{\lambda_1}) - \ln(\tau_{\lambda_2})]}{[\ln(\lambda_1) - \ln(\lambda_2)]}, \tag{8}$$

which, as a ratio of logarithms, is independent of logarithmic base. The parameter $\alpha_{440,870}$ is a standard AERONET product, and from this point all references to α indicate $\alpha_{440,870}$. In the AERONET record a least-squares fit of all AODs within that spectral range is used to calculate α to reduce the impact of noise; otherwise, at low optical depths the uncertainty on direct-Sun τ (of order 0.01; *Holben et al.*, 1998, *Eck et al.*, 1999) can propagate into significant uncertainties on α (see examples given by *Wagner and Silva*, 2008).

The constraints are that $\tau_{500} \leq 0.2$ (where, if not available directly, τ_{500} is estimated from the nearest available AERONET wavelength and α using Equation 8), and that $0.1 \leq \alpha \leq 1$. These eliminate cases where there is likely residual cirrus contamination or some non-maritime component in the aerosol, such as a local or transported pollutant, as pollutants are typically fine aerosol particles with large positive α, while desert dust and cirrus clouds have small or negative α, and the background maritime AOD is typically low (for example *Eck et al.*, 1999, *Kaufman et al.*, 2001, *Dubovik et al.*, 2002, *Knobelspiesse et al.*, 2004, *Smirnov et al.*, 2009, 2011). *Smirnov et al.* [2003a] used $\tau_{500} \leq 0.15$ and $\alpha \leq 1$; in this work, the rationale behind altering the constraints was based on manual inspection of size distributions which revealed that cases where $0.15 \leq \tau_{500} \leq 0.2$ generally still appeared maritime in character (and increased the data volume by approximately 10 %), while the lower bound on α removed a small number of distributions which appeared suspect. However, if the thresholds used by *Smirnov et al.* [2003a] are retained, results are numerically very similar. The remaining retrieved size distributions are classified as 'pure maritime', and the number of such distributions, as well as the proportion of all distributions meeting these criteria, are given in Table 1.

Midway Island has, of the well-sampled sites, the highest proportion (86 %) of retrievals meeting the maritime criteria, and Kaashidhoo the lowest (20 %). The average size distributions for all retrievals, and all retrievals designated pure maritime, calculated in each case from the median $dV(r)/d\ln(r)$ in each size bin, are shown in Figure 2 for these sites. The difference is minimal at Midway Island, which is not surprising. At Kaashidhoo, the coarse mode is not significantly different between the two cases. However, the 'all data' average shows a significantly stronger fine mode contribution (with a peak around 0.2 μm), corresponding to transported continental aerosol. For both sites, the range of $dV(r)/d\ln(r)$ is large, particularly near the fine-mode and coarse-mode peaks.

It should be emphasised that these size distributions still represent a retrieval, rather than direct measurement, of aerosol properties. Due to the selection of low-AOD cases, AERONET-retrieved refractive indices are not reliable in these situations (*Dubovik et al.*, 2000) and so are not considered. Nevertheless, AERONET offers a much greater sensitivity to aerosol parameters than current satellite instruments, and provides the most comprehensive ground-based dataset available, in terms of spatial and temporal coverage, data quality, and consistency of calibration and processing. Additionally, the large sample size, use of medians to decrease sensitivity to outliers (from retrieval error or residual non-marine conditions), and fact that the inversions used pass the AERONET quality control criteria to be raised to level 2 (*Holben et al.*, 2006), mean that the size distributions considered should be suitable for quantitative analysis.

2.2. Properties of average size distributions

For each of the 22 size bins, the median volume density from those inversions meeting the pure maritime criteria has been extracted to define an average size distribution for each site. This is what is meant by the term 'median' or 'average' distribution through this work (i.e. median calculated for each individual size bin, rather than the median total aerosol volume). The use of medians is to limit the sensitivity to outliers. If means are used instead then the results are insignificantly affected at most sites (although the total aerosol volume typically increases, as most of the outliers are of higher-than-average volume). Throughout this work, if a median is taken of a set containing an even number of values then the numerically larger is taken; this choice has a negligible impact on the results. The averaged distributions are shown in Figure 3. The sites all show a similar bimodal distribution, with a fine mode peaking at 0.1-0.2 μm and a coarse mode peaking near 3 μm. Visually it resembles a bimodal lognormal distribution, although the coarse mode is persistently skewed, with a wider tail on the low-radius end. The broad similarity between sites is an indication of the similar origins of the aerosol in different global oceans, although the abundance of both modes can vary, with Ascension Island and Midway Island having notably higher coarse-mode volumes than the other sites. Crozet Island has the smallest aerosol volume, perhaps because of the site's elevation; it is also amongst the most skewed of distributions.

The AERONET level 2.0 inversion product includes estimates of C_v, r_v, and σ_v (as well as r_{eff}) for the overall size distribution, as well as, separately, fine and coarse modes (hereafter denoted by subscripts f and c respectively). However, these calculations follow from Equations 3 and 4, with the separation between fine and coarse modes determined by estimating the inflection point in the retrieved binned size distribution, as opposed to from a fit to an assumed distribution shape. The average of these parameters is given in Table 2 for each site. The uncertainties are given as the scaled median absolute deviation (SMAD) about the median for each parameter,

$$\text{SMAD}(\text{x}) = \beta(\widetilde{\text{x} - \tilde{\text{x}}}), \tag{9}$$

where $\sim$ indicates a median quantity and β is a scaling factor. If the underlying distribution is Gaussian, then the

SMAD is equivalent to the standard deviation for $\beta = 1.4826$, which is assumed here. The use of SMAD rather than standard deviation here is again to reduce the sensitivity to outliers, and so provide a more representative estimate of the variability of the aerosol size distribution parameters in clean maritime conditions.

Given the skewedness exhibited in Figure 3, the averages of the size distribution parameters provided in the AERONET product are not the same as best-fit lognormal distribution parameters from the averaged size distribution. As a distribution constructed from lognormal components is desired, several approaches to addressing this therefore suggest themselves:

1. Use the AERONET-derived parameters from Table 2 directly as bimodal lognormal distribution parameters, even though the underlying distribution is skewed. This will be referred to as the 'AERONET lognormal' method.

2. Fit the average size distribution to a bimodal lognormal distribution. For this method, bins up to and including the inversion point are used to fit the fine mode, and bins with larger r the coarse mode, with a least-squares equal-weighting method. This will be referred to as the 'fitted lognormal' method. Although the bins adjacent to the inversion point may contain volume from both modes, in practice their inclusion or omission was found to have an insignificant effect on the fits.

3. Fit a trimodal lognormal distribution to the retrieved AERONET size distribution, where the larger two modes will represent the skewed coarse mode of a bimodal distribution.

The objective is then to determine which of these methods leads to a distribution whose radiative properties match best those of the (non-lognormal) AERONET observations. The preferred method is the simplest one to match within the uncertainties of the data. Trimodal distributions are not investigated in detail here; succeeding sections of this work will show that a bimodal distribution is sufficient and the added complexity of a trimodal distribution is not required for this particular application (although the addition of modes does, of course, improve the fit to the retrieved size distributions). In the studies cited throughout this work, both bimodal and trimodal aerosol models have been used, although bimodal are the more common. An example of the average retrieved distribution, and multimodal lognormal distributions fit to it, is shown for Lanai in Figure 4. The SMAD of each bin is generally proportional to $dV(r)/d\ln(r)$, which occurs due to changes in $C_{v,f}$ and $C_{v,c}$ for different AERONET observations. This suggests the primary variability between different size distributions is 'up-down' (total volume) rather than 'left-right' (peak position). Using the AERONET distribution parameters directly for a lognormal distribution results in a larger-r fine mode and smaller-r coarse mode peak than the averaged retrieved AERONET distribution. The fine and coarse mode volumes obtained from both methods are very similar. A trimodal lognormal fit is also shown, which provides a very close match to the average distribution.

The lower portion of Table 2 shows the volume size distribution parameters for each AERONET site for a bimodal lognormal fit, along with uncertainty estimates. For both these and the measured parameters provided by AERONET (Table 2), the parameters are close for most sites, particularly those with a high number of AERONET inversions, suggesting that an approach to define a global maritime fine-mode and coarse-mode may be successful. Differences between sites may arise from factors such as differences in typical wind speeds or humidity between the sites (discussed below).

The largest coarse mode radii are found at Nauru. *Henderson et al.* [2006] report that wind-induced wave-breaking leads to sea salt aerosol production in the coastal surf zone, and formation of downwind cloud trails, at this site. It is possible that the larger radii observed by AERONET here arise as a characteristic of this wave-breaking, or the frequent cloud trails mean residual cloud contamination is more likely. *Henderson et al.* [2006] also note that wind at Nauru is predominantly from the east; it is possible that an asymmetric aerosol field could lead to a bias in the AERONET inversion. Because of this strong surf zone source, results at Nauru may be less representative of the open ocean.

The fine and coarse effective radii are 0.132 μm and 1.70 μm for the 'AERONET lognormal' method (i.e. Equation 7 applied directly to AERONET distribution parameters), and 0.122 μm and 1.80 μm for the bimodal lognormal fit, as compared to 0.150 μm and 1.87 μm when calculated from the AERONET distributions directly (i.e. Equation 5). The 'AERONET lognormal' method is therefore closer for the fine-mode effective radius, but the bimodal lognormal fit is closer for the coarse mode. Overall, these distribution parameters (for both methods) are within the range of other studies (such as summarised by *Silva et al.*, 2002, *Smirnov et al.*, 2002, or *Smirnov et al.*, 2003a). As also noted by *Smirnov et al.* [2003a] and *Ahmad et al.* [2010], the AERONET size distributions are narrower than the older models presented by *Shettle and Fenn* [1979].

Table 2 shows both mean and number-weighted-mean size distribution parameters. However, from this point the number-weighted values will be used, such that the influence of poorly-sampled sites which more frequently report outlying values (Kaashidhoo, Amsterdam Island, and Crozet Island) is mitigated. The same conclusions broadly hold if the unweighted multi-site mean is used instead, as the weighted and unweighted means are similar.

3. Relationship with meteorological parameters

3.1. Data source

The results in Table 2 are averages for all conditions. However, it is known (discussed later) that the aerosol loading is influenced by meteorological factors such as the wind speed or availability of moisture. In this section, the data are therefore examined for these relationships. The National Center for Environmental Prediction (NCEP) reanalyses, available at 1° horizontal resolution output every 6 hours, are used for this purpose (*Derber et al.*, 1991). Although coarse-resolution, such model output products are nevertheless the only current source of global spatially and temporally complete meteorological data, and so the only recourse if such information is to be used as an input to a global multiyear satellite aerosol retrieval scheme.

Wallcraft et al. [2009] compared satellite, buoy, and numerical weather prediction (NWP) model (including NCEP) near-surface wind speeds and found each dataset exhibited the same spatial patterns, although with regional relative biases. NCEP was found to have a positive bias relative to QuikScat satellite data of up to 2.5 ms^{-1} in high-wind regions in the storm tracks. However, the correlation with QuikScat was high (greater than 0.9 over most of the open ocean) and bias smaller than 0.5 ms^{-1} in many oceanic regions, including those where most of the sites used in this study are located. The bias and root-mean square difference between NCEP data and buoys were found to be small (0.15 ms^{-1} and 0.97 ms^{-1} respectively). The overall quality of agreement was similar for the different datasets assessed. It is therefore suggested that any of these NWP datasets would provide a reasonable assessment of the near-surface oceanic wind speed near these sites. *Wallcraft et al.* [2009] also note that NWP results are likely to improve for more recent years than the period analysed (1998-2002) due to increased availability of observational data for assimilation.

Figure 5 shows the results of comparisons between linearly spatio-temporally interpolated NCEP wind speed and relative humidity near-surface fields with meteorological data recorded at approximately 10-minute intervals from twelve cruises of the Research Vessel (RV) Polarstern. These cruises are Atlantic Ocean transects, chosen to cover the latitude range inhabited by the relevant AERONET sites, and sampling a wide range of wind speeds (*König-Langlo*, 2005a, 2005b, 2005c, 2005d, 2006, 2008a, 2008b, 2008c, 2009a, 2009b, 2010a, 2010b). Overall the correspondence is high, although the coarser spatial and temporal resolution of the NCEP data mean there is a tendency for extrema to be missed. When the instantaneous wind speeds are averaged to daily values, the gradient of the least-squares best fit line forced through zero does not change much (0.84 to 0.85), i.e. the NCEP data tend to underestimate the wind speed. However, the correlation increases from 0.90 to 0.96. For relative humidity, the data are almost unbiased (gradient 0.97) although the correlation coefficient is lower (0.54), reflecting the typically small variability of relative humidity observed. These results support the validity of the use of NCEP data for the analysis of the relationship of aerosol properties with meteorology. However, the differences underscore the fact that analyses of this type are sensitive to not only the quality of the aerosol data, but also the meteorological data. Part of the discrepancy may be due to the altitude difference (10 m for NCEP, as compared to 25 m above sea level for the ship).

Additional AERONET aerosol products may provide further insight into the relationship between marine aerosol and the ambient conditions. Firstly, although the AERONET size distribution inversions include temporal averages of direct-Sun AODs (as discussed previously), the full direct-Sun dataset is significantly larger. This is because direct-Sun measurements are taken every 15 minutes, while the almucantar scan is performed hourly, and requires completely cloud-free skies in the scanning plane. The second avenue is through the spectral deconvolution algorithm (SDA) data product, which provides the partition of AOD at 500 nm into separate contributions from the fine and coarse mode, and is independent of the other AERONET aerosol retrieval algorithms (*O'Neill et al.*, 2003, 2006 for the current version 4 level 2.0 dataset).

Both of these additional products are therefore considered. As before, the restrictions that $\tau_{500} \leq 0.2$, $0.1 \leq \alpha \leq 1$, and data from 1999 onwards (2010 for Graciosa), are imposed. Additionally, to decrease the noise, and because of the coarser NCEP resolution, after obtaining the meteorological information for each case, the direct-Sun and SDA products are downsampled to daily averages for the comparisons with wind speed and relative humidity before these thresholds are applied. This provides between 125 (Kaashidhoo) and 1,171 (Midway Island) dates per site, with typically around 15 measurements contributing to each daily average. This daily averaging is not done for the size distribution inversions, as these are less frequent (many days have multiple direct-Sun measurements but no size distribution inversions). Additionally, the data are not averaged for the water vapor comparisons, as these are part of the AERONET product and so do not require matching with additional NCEP data.

3.2. Dependence on wind speed

Studies from both satellite and ground-based data have shown that increased near-surface wind speeds (ws) are associated with an increase in AOD, due to wind increasing the flux of sea spray (i.e. increased aerosol mass), and water vapor (i.e. aerosol swelling), from the ocean to the marine boundary layer (recently *Zieliński and Zieliński*, 2002, *Smirnov et al.*, 2003b, *Satheesh et al.*, 2006, *Mulcahy et al.*, 2008, *Sakerin et al.*, 2008, *Glantz et al.*, 2009, *Huang et al.*, 2010, *Lehahn et al.*, 2010, *Adames et al.*, 2011, *Grandey et al.*, 2011, *Kiliyanpilakkil and Meskhidze*, 2011). These are similar to earlier results which directly sampled aerosol particles, rather than remotely-sensed AOD (e.g. *Lovett*, 1978, *Blanchard and Woodcock*, 1980, *Monahan et al.*, 1983, *Exton et al.*, 1985, *Hoppel et al.*, 1990). Stronger wind speeds will, however, mean the aerosol is transported downwind of its source more rapidly, and so simple relationships between the two quantities are unlikely to capture most of the variability in aerosol loading, unless meteorological conditions are homogeneous over a large area and time period, and there are no other aerosol sources.

Stronger correlations have been observed using the wind speed averaged over some time before the aerosol measurements were made ('wind speed history'), rather than instantaneous wind speed, as wind may change on timescales shorter than aerosol lifetimes; the strongest correlations are typically found with wind speed averaged for 12-24 hours prior to the AOD measurement (*Gathman*, 1983, *Hoppel et al.*, 1990, *Smirnov et al.*, 2003b, *Lehahn et al.*, 2010). Some of these analyses bin data by wind speed, and then fit binned averages; this binning will naturally lead to stronger correlations than fits using all data points, as the variability is somewhat averaged-out, so this should be borne in mind when examining regression statistics from different studies. *Mulcahy et al.* [2008] found, for stable wind conditions, a very strong relationship between bin-average AOD and the approximate square of the wind speed. However, this was based upon measurements at a coastal site, and it is possible that breaking waves on the rocky shore would lead to the production of additional aerosol above what would be observed in open-ocean (i.e. rock-free) conditions, or that there are differences in wind conditions between the coast and nearby ocean (*Blanchard and Woodcock*, 1980, *Henderson et al.*, 2006). It is uncertain whether these trends continue for high wind speeds, due to a paucity of data for $ws \approx 10$ ms^{-1} or higher, and the few observations in these conditions have shown either increases, levelling-off, or decreases in aerosol loading in strong winds (*Blanchard and Woodcock*, 1980, *Exton et al.*, 1985, *Mulcahy et al.*, 2008, *Pant et al.*, 2008, *Grandey et al.*, 2011, *Kiliyanpilakkil and Meskhidze*, 2011).

In this analysis, for each AERONET size distribution, NCEP near-surface (10 meter) wind speed data points are linearly interpolated in space and time to provide the 'instantaneous' wind speed. The wind speed history is then defined by repeating this procedure backwards in time in 6 hour increments, and averaging the resulting wind speed for up to 96 hours prior to the time of the AERONET retrieval. Pearson's linear correlation coefficient between aerosol parameters and this time-averaged wind speed are shown in Figure 6, separately calculated using all AERONET data together, and then individually for those sites with 100 or more AERONET inversions. The correlations with the size distribution parameters are calculating using those directly reported by AERONET (i.e. those from which the averages in the upper part of Table 2 were computed) rather than those from lognormal fits; similar results are obtained if the lognormal fit results are used instead.

The strengths of correlations, and the time period which provides the strongest correlation, varies between sites. However, generally all sites show the same sign of correlation between the aerosol parameter and wind speed history. Even if the true response of aerosol to changes in wind speed were the same at each AERONET site, the strengths of correlations might be expected to vary due to factors such as how well the coarse-resolution NCEP data represent the real wind speed; the range of wind speeds observed at a given location (if the response of the aerosol is nonlinear); and the fact that the sites are above sea level, so if a significant

proportion of the aerosol response takes place near the air-sea interface below the site then this may be missed in the AERONET data if the aerosol is not vertically well-mixed. *Blanchard and Woodcock* [1980] present a model for the vertical dependence of sea salt concentration, based on wind speed; according to this, the highest number of particles are found at heights of up to 0.2 m above the sea surface, but most of these particles rapidly fall back in. For heights of meters to several hundreds of meters, there is a small decline with height, with an eventual inversion layer of increasing concentration in the range 300 m to 600 m. Non-sea-salt components were not considered. It is therefore likely that altitude and background aerosol contribute to the differences between sites. The issue is complicated by the fact that the results of *Blanchard and Woodcock* [1980] were collected in cloudy conditions, while the AERONET data are clear-sky; *Blanchard and Woodcock* [1980] note that the salt inversion layer may depend on boundary-layer cloudiness.

Positive correlations are found between the wind speed history and aerosol volume, particularly for the coarse mode, consistent with previously-mentioned studies. This manifests in additional positive correlations with AOD, stronger for τ_{1020} than τ_{440}, and a negative correlation with α, all linked to the fact that the fine mode is more optically-active in the visible, and the coarse mode in the near-infrared. There are also positive correlations between r_v and the wind speed history, while the correlation is positive for the fine mode spread but negative for the coarse mode. These correlations are, however, generally weaker than those observed for C_v, τ, and α, which themselves are typically 0.4 or smaller.

Given the observed correlations, the next step is to examine the size of the response of the aerosol size distribution to wind speed. For this purpose, averaged size distributions (as described previously) have been calculated by binning the AERONET inversions according to the NCEP wind speed rather than by site. Bins have been chosen such that a large number of inversions fall within each, although there were only 67 cases of winds stronger than 10 ms^{-1}, meaning care should be taken when considering results for high winds. Removing the constraints on τ_{500} and α at Lanai and Midway (the most well-sampled sites) does not result in significantly more high-wind points, implying that these imposed constraints are not causing a bias to low wind speeds. Approximately 83 % of inversions were for wind speeds from 4-10 ms^{-1}. The resulting size distributions are shown in Figure 7. Table 3 details the number in each bin, τ, and α, and shows the expected increase of AOD with wind speed and corresponding decrease of α. Size distribution parameters (for both the median of the corresponding AERONET inversion parameters, and lognormal fits to the median of distributions) are given in Table 4. The highest winds have a slightly lower AOD than anticipated by this trend, due to a slight decrease in the fine mode volume, although as mentioned sampling is comparatively poor for this range. The base AOD for the calmest waters appears to be 0.068 at 440 nm and 0.04 at 1020 nm. This is similar to (but slightly higher than) background AOD at 870 nm for dust-free period at Barbados of 0.035-0.04 reported by *Smirnov et al.* [2000b]. The results for typical wind speeds also match well the 'baseline maritime' AOD at 500 nm of order 0.052-0.071 reported by *Kaufman et al.* [2001], if the values in Table 3 are interpolated spectrally, and observations taken on the decks of ships (*Smirnov et al.*, 2011).

It is observed that, as wind speed increases, fine mode properties show mixed trends. The change in $C_{v,f}$ is small, but potentially a decrease as wind speeds increase. The coarse mode exhibits a larger change; $C_{v,c}$ increases strongly with higher winds, consistent with the previously-mentioned studies. The difference between bin averages for the lowest and highest winds is a factor of two. Additionally, $r_{v,c}$ increases, although σ_c varies less strongly. The increase of $r_{eff,c}$ is driven mostly by the changes in $r_{v,c}$.

The difference between $r_{v,c}$ for the two most populated bins (4-6 ms^{-1} and 6-8 ms^{-1}) is within the variability of distributions in each bin (for the 'AERONET lognormal' method) and smaller than the fit uncertainty on each bin (for the 'lognormal fitted' method). The same is true for σ_c. They are also smaller than or comparable to the variability or fit uncertainty of these parameters at individual sites (Table 2). Additionally, the values of these parameters for the 0-4 ms^{-1} and 8-10 ms^{-1} bins are typically within or close to the variability or fit uncertainty. These are important results as they indicate that the multi-site average $r_{v,c}$ and σ_c may be able to represent coarse-mode aerosol for the majority of encountered wind strengths. This highlights again the underlying similarity of the coarse-mode aerosol at different locations (i.e. aerosol found at different locations with similar wind speeds correspond more closely than aerosol observed at a single location over a range of wind speeds). The change in the results of this analysis are small if size distributions are binned by the 24-hour-average, rather than instantaneous, wind speed.

3.2.1. Fits of C_v to wind speed

Linear and exponential fits of AERONET retrieved fine and coarse mode volumes ($C_{v,f}$ and $C_{v,c}$) to the 24-hour-averaged wind speed are shown in Figure 8, for data from all sites considered together. In both cases, the correlation is much stronger for the coarse mode than fine, although both linear and exponential models provide a similar quality of fit, due to a comparative lack of data for high wind speeds where nonlinearity would be more evident in the exponential model. For the most commonly-encountered wind speed ranges, both methods give very similar results. The fine mode volume is independent of wind speed, while the coarse shows a positive correlation, consistent with the mechanism of wind-driven emission. The 24-hour-average wind speed is used as it shows a stronger correlation with aerosol volume than instantaneous wind speed in most cases (Figure 6), although coefficients of fit are similar if instantaneous wind speed is used instead. Similar results are obtained if the fits are performed on a site-by-site basis (omitted for brevity), with the fine mode independent of wind speed and the coarse mode typically with a base volume of 0.01-0.02 $\mu m^3 \mu m^{-2}$ and an increase of order 0.005 $\mu m^3 \mu m^{-2}$ per 1 ms^{-1} wind speed, although the smaller individual sample sizes lead to high uncertainty on fit coefficients.

For the fine mode in Figure 8, high outliers contribute to the fact that the least-squares regression linear intercept (0.0064 μm^3 μm^{-2}) is higher than the average observed fine mode volume for a lognormal distribution (0.0057 μm^3 μm^{-2} or 0.0056 μm^3 μm^{-2}, from upper and lower portions of Table 2). For these very low $C_{v,f}$, least squares regression is less appropriate as the spread of values may not be Gaussian (i.e. the AERONET data will not retrieve a negative volume; thus, noise on the low-volume retrievals will be on average biased positive). If an alternative fitting method than least-squares is used, such as least absolute deviation (*Bloomfield and Steiger*, 1980) or reduced major axis (*Ayers*, 2001), then the fine-mode fit parameters change (although correlations remain effectively zero) while coarse mode fit parameters are affected minimally in most cases.

Averaging the data over all sites in bins of 0.5 ms^{-1} provides significantly stronger correlations, as shown in Figure 9, for linear relationships between wind speed and C_v (equations of fit shown in the Figure). To reduce the effect of outliers, bin medians rather than means are used. Several bins at very low and high winds contained very small numbers of retrievals, meaning the bin averages were noisy, and as these bins lie at the edges of the range they have a

strong influence on the linear least-squares fit. For this reason, bins with fewer than ten size distributions have been excluded from the analysis in Figure 9. For the fine mode, quantisation in the AERONET C_v (increments of 0.001) is evident in the fit. Between the quantisation and variability within each bin, there is effective no relationship for the fine mode.

These results imply that, if only the wind speed or wind speed history is known, assuming $C_{v,f} \approx 0.0056$ (i.e. the average observed value) and $C_{v,c} \approx 0.02 + 0.0025ws$ or $C_{v,c} \approx 0.015 + 0.0036ws$ (i.e. the global average best linear relationship for the binned data, dependent on whether instantaneous or 24-hour-averaged wind speed is known) will give a reasonable first-order estimate of the aerosol volume. This is examined further in Section 5. Despite this, wind speed alone is likely to be a poor predictor of aerosol volume; the variability within bins on Figure 9 is similar to the range of volumes encompassed by the best-fit line. Further, the different gradients of coarse-mode volume with wind speed presented in this section vary by a factor of two, as a result of simply changes in data aggregation. The data do not permit analysis for very high wind speeds. To an extent this will be related to inadequacies in the NCEP data representing the true wind speed history at each site, and errors in the AERONET size distribution retrievals. However, this highlights the necessity for complexity and consideration of the aerosol life cycle from emission to removal in modelling of the aerosol burden, as is performed by the current generation of global models.

3.2.2. Fits of AOD to wind speed

Statistics of linear fits of direct-Sun AOD and α to wind speed (in both cases, from points averaged for each day) are presented in Table 5. There is considerable variety between the sites, both in terms of strength of correlation and the fit parameters, which may in part reflect different local sources. In general, the strongest agreement is found between ws and α; stronger correlations are found with τ_{1020} than τ_{440}. These results can again be explained in terms of an increased coarse-mode presence at higher wind speeds. Due to the high scatter, the uncertainties on these linear fit parameters (not shown) are large. There is effectively no significant correlation between $\tau_{500,c}$ and wind speed. Although this is a surprising result, because the coarse mode optical depth at this wavelength is low (as compared to 1020 nm, where almost all the AOD comes from the coarse mode), it is likely that any signal is masked by the uncertainty on $\tau_{500,c}$ and wind speed, or background variability. Another possibility is uncertainties in the fine/coarse partition in the SDA data. The relationship between $\tau_{500,f}$ and wind speed is similar to that of τ_{440}; this can be explained by the fact that AOD at 440 nm is mostly determined by the fine mode, so τ_{440} and $\tau_{500,f}$ are sensitive to the same parts of the underlying aerosol burden.

Averaging the data over all sites in bins of 0.5 ms^{-1}, and taking the bin medians, leads to the relationships shown in Figure 10. Again, poorly-sampled bins (fewer than 10 points) are omitted. An approximate linear relationship appears to hold for all cases, although the largest outliers on the fit occur for wind speeds higher than 12 ms^{-1}. As in the case for aerosol volume, the variability within each bin is similar to or larger than the range of the bin-average values, again illustrating that wind speed alone is of limited utility in predicting the marine aerosol burden for an individual case.

3.2.3. Joint analysis with sea surface temperature

Marine (sea spray) aerosol source functions in Earth system models are typically the product of an assumed size distribution with a (wind-speed-dependent) fractional whitecap cover, although there is considerable scatter between different parametrisations (*Lewis and Schwartz*, 2004, *O'Dowd and de Leeuw*, 2007). *Jaeglé et al.* [2011] improved the correspondence between modelled and observed sea salt aerosol burdens by modifying the source function of *Gong* [2003] with an empirical sea surface temperature (SST)-dependent correction. This dependence is thought to arise partially due to the changing kinematic viscosity of the sea surface with temperature (determining bubble rising and breaking), and may also partially be because observed whitecap fraction is also linked to SST (*Anguelova and Webster*, 2006). An SST dependence has also been observed in laboratory studies of seawater and analogues (*Sellegri et al.*, 2006, and references therein).

Due to diurnal changes in SST, aerosol lifetimes on the order of days, and the fact that the AERONET sites are not located at the ocean surface, the observed aerosol in the atmosphere at any given time may not be representative of the aerosol flux from the ocean for the temperature at that given time, and there is no direct match possible between SST and the AERONET inversions. For these reasons, the version 2 Optimal Interpolation (OI) SST dataset (*Reynolds et al.*, 2006) is used for a joint analysis of effect of wind speed and SST on aerosol. This provides global gap-filled, bias-corrected, daily average (daytime and nighttime orbits) bulk SST. As the SST is bias-corrected against buoys, this bulk SST corresponds to a depth of order 0.5 m below the surface, and is typically within 0.5 K of the skin SST, although this depends on meteorological factors (e.g. *Murray et al.*, 2000). The dataset is derived from Advanced Very High Resolution Radiometer (AVHRR) and Advanced Microwave Scanning Radiometer (AMSR) data. It is provided on a 0.25° grid but here is downsampled to 2.5° resolution to provide a better representation over the larger source region that the AERONET site may sample from on a given day.

The mean SST is 24.5°C (median 24.7°C), and the standard deviation 2.9°C. The coolest and warmest temperatures encountered are 4.2°C and 31.0°C respectively, although the number of cases with water cooler than 20°C is very small. This is because the majority of the sites are in warm tropical waters, and so any conclusions drawn may be unrepresentative of cooler waters.

Figure 11 is analagous to Figure 7, except the data are also subdivided by SST. The 24-hour-averaged wind speed has been used to stratify the data, although the results do not change significantly if the instantaneous wind speed is used instead. The SST bins have been chosen to be narrow while still retaining sufficient sampling in as many cases as possible, although this is difficult for the highest wind speeds ($ws > 10$ ms^{-1}). Despite the previously-documented links between SST and marine aerosol production, there appears no strong and consistent link with the size distribution here (certainly compared with the effects of wind speed). For high winds, the coolest (SST< 21°C) and warmest (SST> 27°C) have a higher coarse-mode volume than the intermediate SST ranges, although the sample size for these wind and SST bins is very limited, so these results should be interpreted with caution.

Given the rough linear relationship between wind speed and coarse-mode volume observed in the previous section, and the results of *Jaeglé et al.* [2011] that scaling the source function for marine aerosol production by a cubic polynomial in SST improved the marine aerosol burden in a global model, similar fits (omitted for brevity) of the form $C_v = (a + b\mathrm{SST} + c\mathrm{SST}^2 + d\mathrm{SST}^3) \times (e + f \times ws)$, where $a - f$ are coefficients to be determined, have been attempted here, for fine and coarse mode volume. However, using such fits Pearson's linear correlation coefficient showed only slight improvement as compared to the wind-speed-only relationship for both fine and coarse modes, strengthening from 0.03 to 0.12 and 0.38 to 0.42 respectively. These results suggest that consideration of SST provides minimal additional skill

in predicting marine aerosol loading. This may reflect uncertainties in how well the datasets (AERONET, wind, and SST) are able to represent the true aerosol or meteorological conditions, or simply that although SST may affect aerosol production, aerosol lifetime is sufficiently long that it has little impact on the total aerosol burden in these regions. The SST range sampled may be a significant factor, given that the largest corrections to the aerosol source function made by *Jaeglé et al.* [2011] are outside the typical range of AERONET data used here.

3.3. Dependence on relative humidity

Historically, a common approach to modeling aerosol size distribution and refractive index, such as in the frequently-used database of *Shettle and Fenn* [1979] and those which draw from it (e.g. *Hess et al.*, 1998), has been to initially define properties for a 'dry' aerosol type of some assumed composition. These 'dry' properties are then modified according to variations in relative humidity (rh) using models of aerosol swelling (e.g. *Hänel*, 1976, *Kotchenruther et al.*, 1999 for marine cases). The effect of this is, as the relative humidity increases, the size distribution shifts to larger particles and the refractive index approaches that of water, with the change dependent on composition. As the size distributions in this work are calculated from AERONET inversions they represent the aerosol size distributions as found 'in the wild', and their variability will encompass the effects of the range of relative humidity and consequent aerosol swelling and drying. There are difficulties when trying to use a method based on knowing the relative humidity to define an aerosol model. Analogously to wind speed, the quality at which coarse-resolution model relative humidity is able to represent the actual relative humidity on a finer scale is likely highly variable. Aerosol swelling shows hysteresis, such that even if the relative humidity were known this may not be sufficient to model the extent of swelling unless the prior history of the air mass is also known (*Kotchenruther et al.*, 1999). Additionally, there is evidence that in the case of sea salt aerosol the currently-used mixing rules do not reproduce the observed refractive index (*Irshad et al.*, 2009). Finally, it should not necessarily be expected that the AOD should correlate well with near-surface humidity, as AOD is a columnar quantity.

NCEP rh data are interpolated here to AERONET inversions in the same way as the wind speed data. There is little direct correspondence between the relative humidity and wind speed (not shown), and the interval $60 \leq rh \leq 80\,\%$ contains 88 % of all relative humidities encountered. Figure 12 shows the averaged AERONET size distribution (calculated as previously) for inversions aggregated by relative humidity; Table 6 shows the number of retrievals in each bin, as well as τ, α, and the mean wind speed for the data in that bin (which is similar for each, varying by 1.7 ms^{-1} or less between bins). Table 7 gives statistics of these distributions and fits to them, in the same way as Table 4 for wind speed.

Some studies have observed an anticorrelation of τ and rh for rh <75 %, and a positive correlation for rh >75 %, when measured simultaneously on ships (*Smirnov and Shifrin*, 1989, *Smirnov et al.*, 1995). This was attributed to turbulent exchange in the marine boundary increasing τ and decreasing rh, leading to a natural anticorrelation, but this effect being overwhelmed by moisture uptake for high humidities (with a deliquescence point at $rh \approx 75\,\%$, dependent on temperature and composition). Upon first examination, the combination of AERONET and NCEP data provide some evidence to support this relationship. The AOD at 440 nm and 1020 nm, as well as $C_{v,c}$, decrease with increasing rh until around rh =60 %. For rh >90 % they (and $C_{v,f}$) jump dramatically. Other size distribution parameters change less dramatically (except for the most extreme, and most poorly-sampled, bins). This behaviour is consistent with increased turbulence leading to increased particle number (but little change in particle type) in 'dry' conditions, but rapid aerosol swelling in 'moist' conditions. There is an increase of α with rh up to rh =85 %, and then a drop. The drop in α for the lowest and highest humidities could be related to the swelling of aerosol but could also be an artefact of cloud contamination or limited sampling. The variability of α within most bins is large.

However, the evidence is weak, because of the poor sampling for low and high humidities. In particular there are only four cases of rh >90 %, and the average size distribution is unusual compared to the other ranges. The fact that these are grid-box average humidities suggests the presence of clouds in some region of the grid box is likely, and so it may be that these distributions are unphysical and contaminated by clouds. All four of these cases occur for Graciosa, from which the data have not yet been raised to level 2.0 (i.e. full quality control has not yet been applied). Similarly, for the range $80 \leq rh \leq 85\,\%$, 27 of the 38 points are from Graciosa. Of the 71 points with rh <60 %, 40 occur at Midway Island, 19 at Lanai, and 6 at Bermuda. Midway Island and Bermuda can on occasion be influenced by transported dust (*Smirnov et al.*, 2000b, 2003b) and so Lanai may also. It is therefore possible that the low-humidity results here are influenced by dust transported in dry air masses, rather than a change in the abundance of marine aerosol. All of these points at Midway occur from December to April, when dust transport is expected to be most likely. If points from Midway and Lanai are removed, then for rh <60 % the mean τ_{440}=0.068, τ_{1020}=0.047, and α=0.38, although sampling becomes very poor. In these cases the AODs and size distributions for low humidities match closely those for other humidity ranges (except the suspect Graciosa rh >90 % data) in Table 6, and the trend in AOD with rh is effectively removed, although the trend in α remains. Removing the Bermuda data does not have a significant effect on the results. It is therefore possible that this small number of the driest cases represent residual contamination by transported dust. The coarse-mode peak radius is also shifted to larger volumes for these drier bins, which supports this (Figure 12). If these seasons are removed for these sites for the previous main analysis of aerosol size distributions (Section 2.2), however, the impact is negligible.

Some of the variability in all these cases will arise from the hysteresis of aerosol deliquessence (i.e. the path by which the current relative humidity was reached is important), which may mask any change in aerosol properties expected around rh =75 %. Inadequacies in the coarse-resolution NCEP data will also limit the extraction of useful information. Over the heavily-populated range $60 \leq rh \leq 80\,\%$ size distribution parameters show little change, suggesting that average values are sufficient to describe the majority of cases encountered. The sampling is inadequate to make confident statements about behaviour in low or high humidities. To further examine these relationships between relative humidity and AOD for dry and moist air, linear regressions have been performed using the direct-Sun data. Binning daily average data from all sites together (as in Figure 10 for wind speed) leads to Figure 13, the trends of which are broadly consistent with Table 6, although again the variability within each bin is typically larger than the range spanned by bin-median values. Sampling is insufficient to examine data for rh >90 %. The same conclusion is reached if other wavelengths are used; whether the data are subset according to wind speed or not; whether instantaneous or daily-averaged data are used; or whether sites are considered individually or jointly.

3.4. Dependence on water vapor content

In addition to the aerosol bands, the Sun-photometers used in AERONET have a channel around 940 nm which enables the retrieval of water vapor with an uncertainty of order 5 %-10 % (*Smirnov et al.*, 2004, *Alexandrov et al.*, 2009).

This provides an alternative way to examine the effect of moisture on maritime aerosol. The columnar water vapor is provided in units of g cm^{-2} (equivalent to cm, given a density of 1 g cm^{-3}). Separating the AERONET size distributions according to columnar water vapor gives average distributions shown in Figure 14. The lowest bin ($0 \leq wv \leq 1$ cm) has the lowest volume (and AOD), but aside from that there is no significant dependence of distribution parameters on water vapor content (tables omitted for brevity). Table 8 shows the variation in AOD with columnar water vapor, along with the average wind speed for each bin; there is no trend. The case of the $0 \leq wv \leq 1$ cm bin is sampled poorly, and approximately half (7/15) of the size distributions are from Crozet Island, so in this case the low AOD and water vapor may both be due to conditions specific to this site rather than an effect of water vapor on AOD. It is therefore likely that results for this water vapor range do not represent open ocean conditions well. There is a small increase of α with water vapor; however, the variability on α within each bin (0.15-0.2) is of similar size to the range over all bins.

The relationship has also been examined for individual sites, and restricted to different subsets of wind speeds, to investigate whether aggregating data from multiple sites or wind regimes together was masking the signal. However, this did not reveal any significant relationships. The lack of correlation could be explained as a combination of effects resulting from the low ranges of AOD and water vapor encountered; that the vertical distributions of aerosol and water vapor have small overlap thus limited potential for influence; or the possibility that the timescales of aerosol growth and water vapor variability are different. This site-dependent relationship (or lack thereof) between AOD and moisture has been noted in previous studies (*Exton et al.*, 1985, *Hoppel et al.*, 1990, *Smirnov et al.*, 1995, 2000c, *Holben et al.*, 2001, *Sakerin et al.*, 2008).

The strength of the linear correlation coefficient R between water vapor content and AOD for direct-Sun data is 0.2 or less in most cases when calculated for any site or wavelength, for a selection of assumed relationships (linear, quadratic, or exponential). This confirms the results from the smaller AERONET inversion dataset that the influence of water vapor on AOD in these pure maritime conditions is small. In case the restrictions $\tau_{500} \leq 0.2$ and $0.1 \leq \alpha \leq 1$ were masking the true relationship (by removing those points where elevated water vapor was associated with an increased AOD), results without these two constraints have also been examined. However, the relationships remain weak; an example is shown for Lanai and Midway Island in Figure 15, for exponential fits between wv and $\tau_{f,500}$ or $\tau_{c,500}$. At Midway Island there is evidence that enhanced water vapor corresponds with a decrease in AOD. This could be related to periodic transport of Asian dust in dry air masses (*Smirnov et al.*, 2003b, *Eck et al.*, 2005) rather than an effect of water vapor on marine aerosol. Also shown in Figure 15 are analagous results for the AERONET sites of Wallops (coastal; 37.942° N, 75.475° W) and COVE (a platform 25 km from the coast; 36.900° N, 75.710° W). Because of their coastal (rather than remote island) locations they are more susceptible to continental influence, which is reflected in the higher AODs than observed at sites like Lanai or Midway Island. For both the 'all points' and 'maritime conditions' datasets, there is a significant strong exponential relationship between AOD and water vapor content, with $R = 0.63 - 0.77$ for fits to all points, and $R = 0.2 - 0.44$ for only those classified as maritime conditions, which is still stronger than most of the relationships found for the sites considered for this study (Table 1). This provides further evidence that the lack of correlation observed for the maritime sites under maritime conditions is real.

3.5. Other factors

Various studies have shown that the organic content of submicron marine aerosol is increased in waters with high biological activity, signified by the enhancement of organic carbon within sea water (such as *O'Dowd and de Leeuw*, 2007, *Fuentes et al.*, 2010), although the relationships are complicated. *Fuentes et al.* [2010] found, for experiments with seawater proxies enriched with algal species, that the number of generated aerosol particles of modal dry radius of approximately 0.02 μm was increased by up to approximately a factor of two as compared to a proxy without the algae. The effect on particles of dry radius of order 0.05 μm and larger, which compose the bulk of the volume of the fine mode, and so fine mode optical depth, was smaller. Therefore it is unlikely that this enrichment has a strong effect on the visible AOD. Additionally, investigation of the effect on the size distribution using AERONET aerosol and satellite organic activity proxies (e.g. chlorophyll-a) data is difficult, for reasons including the physical separation between the Sun-photometers and the water, the possibility for confounding effects from errors in atmospheric correction in the ocean colour products, and the heterogeneity and difficulty of retrieval of ocean colour products in coastal waters. For these reasons, the relationship is not examined here.

Some other factors influencing marine aerosol production are discussed by *Lewis and Schwartz* [2004], but are either difficult to assess using available data, or likely to have a minor influence on the AOD, and so are not further considered here. These include atmospheric stability, precipitation, surface-active materials (such as the aforementioned organic carbon), wave state, boundary layer height, fetch, salinity, and bottom topography.

4. Refractive index and calculated AOD

As well as the size distribution, knowledge of the complex refractive index $m = n - ik$, where n is the real component and k the absorption coefficient, is required to calculate the AOD at given wavelength. Although provided in the AERONET record, for the low AODs considered here the uncertainty on this is large and so results may be unreliable (*Dubovik et al.*, 2000). Additionally, the inversion provides a single refractive index for the aerosol model as a whole. Observational evidence suggests that the fine mode is composed predominantly of a mixture of sulphates, organic compounds, and salt, while the coarse mode is predominantly salt, although the exact composition is variable and dependent on meteorological and biological factors (*Hegg et al.*, 1997, *Magi et al.*, 2005, *Clarke et al.*, 2006, *O'Dowd and de Leeuw*, 2007, *Fuentes et al.*, 2010). These different compositions would be expected to lead to difference refractive indices for the two modes. For these reasons, a variety of refractive indices are tested in this work, shown in Table 9, which includes ground-based observations as well as one pair of components used in the current Moderate Resolution Imaging Spectroradiometer (MODIS) aerosol retrieval over ocean (*Remer et al.*, 2006), and the Optical Properties of Aerosol and Clouds (OPAC) database (*Hess et al.*, 1998), which is drawn from *Shettle and Fenn* [1979], and used in various other satellite and model datasets (e.g. *Sayer et al.*, 2010). This is by no means an exhaustive list, although it does encompass the range of commonly-used values; for example, *Fraser et al.* [1997] use $m = 1.38 - 0.001i$, intermediate between *Smirnov et al.* [2003a] and *Silva et al.* [2002] in Table 9. Although the refractive index has spectral behaviour, over the range of interest here most studies in Table 9 use a broadband value, as variation through the visible and near-IR is small.

The refractive indices and size distribution fitting method are tested by attempting to recreate each case of AERONET

spectral AOD using Mie theory and the multi-site average size distribution parameters $r_{v,f}$, $r_{v,c}$, σ_f, and σ_c from both fitting methods (Table 2). The distribution volumes $C_{v,f}$ and $C_{v,c}$ for each case are taken from the AERONET-reported parameters (or a lognormal fit to the size distribution, as described previously) for each individual observation. In this way the tests mimics the way the average model may be implemented in satellite retrieval schemes, i.e. the spectral AOD is determined only by altering the volumes of each component while the distribution peak radius and spread are held constant. This allows an assessment of the degree to which the average model is able to represent maritime aerosol at each site, and will inherently include the effects of changes in wind speed, relative humidity, and errors resulting from potential aerosol nonsphericity.

For each site, the correlation coefficient, median bias (calculated - AERONET observed AOD), and SMAD are calculated. The evaluation of each combination of size distribution and refractive index, however, is restricted to only five sites in Table 1 with at least 100 observations meeting the maritime criteria (Lanai, Bermuda, Midway Island, Ascension Island, and Tahiti), as these each provide a representative dataset of maritime aerosol data of reasonable size. Although Graciosa and Nauru also have over 100 observations, the former is omitted due to potential concerns about cloud-contamination, and the latter additionally due to suspected influence of surf-generated aerosol (*Henderson et al.*, 2006). Over this subset of sites, the minimum, maximum, and median of each of these parameters is presented for each case in Figure 16. This provides a simple reference of how well each potential combination of size distribution and refractive index is able to represent the AERONET AOD.

Figure 16 reveals that, in general, the spread of statistics between sites is larger than the spread induced by changes in refractive index. All models tends to overestimate α, due to τ_{440} being comparatively unbiased while the AOD at longer wavelengths has a slight low bias. For the purpose of satellite AOD retrievals, this is not likely to be a problem as the bias could simply be redressed by altering the total volume of the fine and/or coarse modes. However, this would mean that the bias would translate from AOD into volume, which would then mean that derived aerosol mass estimates may be inaccurate.

The 'fitted lognormal' approach results in higher correlations between calculated and AERONET AOD, with a lower spread of difference (SMAD). The correlation coefficients are high in all cases, particularly considering that the range of AOD is small (most data are for $0.03 \leq \tau \leq 0.08$). In contrast, this method leads to slightly more negative biases in AOD. These biases typically remain smaller than the SMAD, and importantly both of these are often around the reported uncertainty on AERONET AOD of 0.01-0.02 (*Holben et al.*, 1998, *Eck et al.*, 1999). The SMAD is the metric of most interest because it provides information on the scatter of the AOD about this bias. For these reasons, the 'fitted lognormal' method is deemed the more useful of the two approaches. This is an important result because it demonstrates that, just by varying the volume of each component, a single value of each of $r_{v,f}$, $r_{v,c}$, σ_f, and σ_c are able to reproduce the AERONET AOD over a variety of oceans, wind speeds, and humidities, with a precision similar to that of the AERONET AOD measurements themselves, and even considering the fact there may be a non-maritime contribution to the aerosol loading in some cases.

There is no clear 'best case' of refractive indices to choose. An examination of Figure 16 reveals that all cases tend to underestimate AOD from 675 nm onwards; for this wavelength, the majority of the calculated AOD comes from the coarse mode, while τ is fine-dominated at 440 nm, and both modes contribute approximately equally at 500 nm (calculations not shown). The similarity of the AOD bias for all refractive indices for the longer wavelengths reveals that coarse-mode AOD is (over the range of typical refractive indices listed in Table 9) comparatively invariant with refractive index, which implies that choice of refractive index is probably not significant for background coarse-mode marine aerosol. Conversely, for the fine mode those cases with a larger refractive index (2, 4, and 5, using *Remer et al.*, 2006 and *Shettle and Fenn*, 1979/*Hess et al.*, 1998) result in a higher AOD (and so less negative bias) at 440 nm and 500 nm. However, this means they provide a larger overestimate of α. Given the low AODs encountered, this overestimate of α is not considered problematic, as large errors in α can propagate from smaller errors in AOD (*Wagner and Silva*, 2008). Unfortunately, the AOD is not measured at longer wavelengths at these sites, which means the applicability of the model (and any spectral behaviour of refractive index) at other common satellite wavelengths, such as 1.6 μm and 2.1 μm, may not be assessed directly.

Based on these factors, from this point case 4 from Table 9 (fine mode $m = 1.415 - 0.002i$, coarse mode $m = 1.363 - 3 \times 10^{-9}i$) is used, although results change minimally if case 5 is used instead, or case 2 (for wavelengths of 675 nm or longer). The correlation, median (calculated - AERONET) bias, and SMAD for each site for this choice of refractive index, and the recommended 'lognormal fitted' distribution approach, are provided for τ_λ and α in Table 10. These refractive indices (with size distribution component parameters $r_{v,f} = 0.157$ μm, $r_{v,c} = 2.58$ μm, $\sigma_f = 0.50$, $\sigma_f = 0.72$) are hereafter referred to as the 'recommended maritime model'. The single scatter albedo is approximately 0.98 over this wavelength range.

The site with the most negative bias in AOD (for all refractive index cases) is Kaashidhoo; however, as discussed previously, this site is particularly poorly-sampled, and subject to potential seasonal influences of aerosol outflow from the Indian subcontinent, and so likely less representative of clean maritime conditions. The next-largest biases are for Graciosa, which may also potentially be influenced by transported continental or local pollution, or cloud contamination, as discussed previously. For both of these sites it is likely that a pollutant would be more absorbing than the background maritime aerosol, such that the maritime model would underestimate the fine-mode absorption AOD, which is consistent with the observed underestimates. Crozet Island has the largest scatter, although with a sample size of only eight, is very susceptible to outliers. The low AODs and high scatter at Crozet Island mean that α is reconstructed poorly.

The calculations have also been performed for AOD at 340 nm and 380 nm (and are included in Table 10) which, although not used for the AERONET inversion, are available for parts of the record. The results for these wavelengths are omitted from Figure 16 as they are very similar to those at 440 nm, with spectral trends continued (e.g. stronger negative biases at Kaashidhoo). No additional insight into the most suitable refractive index is obtained. Additionally, when shorter wavelengths are considered the assumption of a spectrally-neutral refractive index is also likely less appropriate.

5. Prediction of Maritime Aerosol Network AODs

The previous sections have focussed on results obtained for coastal island sites. The Maritime Aerosol Network (MAN) component of AERONET (*Smirnov et al.*, 2009) provides spectral AOD measured on ocean cruises using hand-held Microtops II Sun-photometers, with an uncertainty of approximately 0.02 (*Knobelspiesse et al.*, 2004). The AOD is reported at a selection of wavelengths (440,

500, 675, and 870 nm for the cruises used here). Using these data helps to establish the utility of the wind-speed-dependent relationships observed in previous sections. For this analysis, level 2.0 (cloud-screened and quality-assured) AODs from the 'series-average' product are used. One measurement series is defined in this product as the set of AOD measurements taken with a gap of no more than 2 minutes between an individual pair.

A subset of cruises whose measurements took place in areas likely to have minimal influence from transported aerosol sources are used. These are the SA Agulhas (during 2007-2008), Knorr (during 2008), Marion Dufrene (a cruise from each of 2008, 2009, and 2010), Sonne (during 2009), and Astrolabe (during 2009-2010). The MAN data are subject to the $\tau_{500} \leq 0.2$ criterion to improve the likelihood that the aerosol sampled is pure maritime in origin; because of the larger uncertainty on MAN AODs than those from the on-land AERONET sites, the range of permitted Ångström exponents is extended to $-0.1 \leq \alpha \leq 1.2$. Unfortunately, many points remain in coastal or continental outflow regions, such that some contamination by a non-maritime component is likely. To reduce this, it is further required that the measurement be at least 5° from land. This leaves 135 potential cases for comparison (only 104 include AOD at 440 nm).

Next the recommended aerosol size distribution parameters and refractive index as outlined above ($r_{v,f} = 0.157$ μm, $r_{v,c} = 2.58$ μm, $\sigma_f = 0.50$, $\sigma_f = 0.72$, fine mode $m = 1.415 - 0.002i$, coarse mode $m = 1.363 - 3 \times 10^{-9}i$) are used with the relationships $C_{v,f} = 0.0056$ and $C_{v,c} \approx 0.015 + 0.0036ws$ to predict the MAN AOD and α. Statistics of the resulting comparison are shown in Table 11, and a scatter plot in Figure 17. Correlation coefficients are between 0.43 and 0.54 for spectral AOD, which, although low, are significant, and reflect the low range of AODs as well as the high variability of aerosol volume within a single narrow wind speed bin previously observed in Figure 9. The SMAD is of similar magnitude to the uncertainty in MAN AOD. Because of all these reasons, α is poorly-reproduced overall. The majority of predicted AODs are within the MAN uncertainty. The wind-speed relationship tends to slightly overestimate the AOD for low MAN AODs, and underestimate for high man AODs. This could imply either a stronger wind-AOD relationship over the open ocean than at the AERONET sites, or that some of the higher-AOD MAN observations do have a residual non-marine component. An alternative could be differences between the aerosol properties for coastal and open-ocean regions, although this cannot be assessed as the MAN record does not permit retrievals of aerosol size distribution. Performance is similar if the other relationships between wind speed and volume from Section 3.2.1 are applied instead. The main conclusion from this is to confirm that the wind speed alone is not able to predict the instantaneous aerosol burden well over the world's oceans, although it can provide a typical background value.

6. Lidar ratios

Lidar provide a useful tool for examining the vertical structure of aerosols and clouds, which is not readily accessible from radiometers to the same extent. To convert the backscattering measured by a lidar from a particular altitude range into an extinction (which can then be integrated vertically to determine the optical depth), the lidar ratio S, which is a function of aerosol type and wavelength, is required. This can be calculated as

$$S = \frac{\int_0^\pi P(\theta) d\theta}{P(\pi)\omega_0} \quad (10)$$

where $P(\theta)$, the scattering phase function, is typically normalised to integrate to either 1 or 4π, and ω_0 is the aerosol single scattering albedo; i.e. S is simply the ratio of total extinction to backscatter. Wavelength-dependence is omitted in the above for clarity. As such for a given vertically-integrated backscatter, the calculated AOD is directly proportional to S. Depending on the characteristics of an individual lidar, S is either calculated from measured extinction and backscatter (for example, *Pedrós et al.*, 2010), or prescribed as a function of aerosol type. In the latter situation the choice of an appropriate S is therefore important for the accurate calculation of aerosol loading. The Cloud-Aerosol Lidar with Orthogonal Polarisation (CALIOP) sensor has flown as part of the A-Train satellite constellation since 2006, and measures backscattered radiation at 532 nm and 1064 nm (as well as depolarization at 532 nm); the lidar ratios used in the current processing are given by *Omar et al.* [2009]. For unpolluted marine aerosol, these are 20 at 532 nm and 45 at 1064 nm. Table 3 of *Cattrall et al.* [2005] provides a summary of some results from the literature, with mid-visible S for marine aerosol between 24 and 39. Their results also show little spectral dependence. *Ackermann* [1998] performed calculations based on the OPAC database, giving S in the range 25-30 at 532 nm and 40-60 at 1064 nm for typical relative humidities. *Müller et al.* [2007] summarise a set of field campaigns, in which S at 532 nm was found to be from 23-29 for marine aerosol. *Pedrós et al.* [2010] obtained median values of S at 532 nm of 31, 36, and 37 for air masses originating from different oceanic regions, although there may have been a local contribution to these results. Results from Lanai for the AERONET analysis of *Smirnov et al.* [2003a] give 34.5 at 500 nm and 37 at 1020 nm.

Lidar ratios from distributions obtained in this study are presented in Table 12 for the commonly-used wavelengths of 532 nm and 1064 nm, and are in the range 25-35. Because the bimodal lognormal fits do not reproduce perfectly the retrieved AERONET size distributions, two sets of calculations are presented. All of these assume the refractive index $m = 1.415 - 0.002i$ (fine mode) and $m = 1.363 - 3 \times 10^{-9}i$ (coarse mode). The first set uses the bimodal lognormal distribution parameters for the recommended aerosol model (Section 4), together with bimodal lognormal fits for the distributions binned by wind speed (lower part of Table 4). The second uses the averaged size distributions directly, rather than lognormal fits to them. This makes the assumptions that the volume of particles outside the range of the bins is negligible (supported by Figure 3), and that the cutoff radius between fine and coarse mode (to determine which refractive index to use) is 0.4 μm, which is close to the inflection point in Figure 3. If the cutoff radius is changed in the region $0.3 \leq r \leq 0.5$ μm, S changes by approximately 1 %, so sensitivity to this assumption is small. Additionally, as the recommended model was determined by the weighted average of lognormal fit parameters (rather than a fit to a weighted spectrum), results for Lanai are included in this second case (see Figure 4), as the site with the best sampling. This latter method is expected to yield more accurate lidar ratios, as it uses the retrieved size distributions directly.

Use of exact distributions rather than lognormal fits result in lidar ratios higher by approximately 10 % at both wavelengths. This difference is due to the fact that the size distributions are not perfectly bimodal lognormal. The results are in good agreement with the ranges of the previously-cited studies; they are, however, significantly higher at 532 nm (lower at 1064 nm) than the values used in CALIOP processing (20 at 532 nm and 45 at 1064 nm; *Omar et al.*, 2009). This is an important result as applying a lidar

ratio of 30 as opposed to 20 for CALIOP at 532 nm would increase the unpolluted marine aerosol loading by 50 %; this would explain the relative low bias of CALIOP marine AODs at 532 nm as compared to other datasets over the ocean (*Kiliyanpilakkil and Meskhidze*, 2011, *Oo and Holz*, 2011). The difference at 1064 nm is of similar magnitude but opposite sense (i.e. CALIOP lidar ratio around 50 % larger than the results here suggest). There is a slight decrease of lidar ratio with wind speed; the change is typically 10 % or less from the average value. This provides an estimate of the error which would arise from the assumption of a wind-speed-independent lidar ratio.

If $m = 1.37 - 0.001i$ is used (as in *Smirnov et al.*, 2003a), S increases by approximately 10 % at 532 nm and less at 1064 nm. The highlights the sensitivity to the assumed refractive index. Additionally, the AERONET retrievals do not provide information on the vertical profile of the aerosol, provided a column-integrated amount. Therefore a strong vertical inhomogeneity in particle number or size may lead to errors in the retrieved size distributions, and influence the calculated S. Conversely, if there is significant vertical inhomogeneity in the aerosol size distribution or composition, the assumption of vertically-constant S will be inappropriate when trying to estimate total extinction from a lidar.

7. Conclusions

When aerosol size distributions retrieved at 11 island AERONET sites spread throughout global oceans are filtered to extract data likely representative of unpolluted marine aerosol, the resulting size distributions are similar, with the chief differences between sites being in the total fine and coarse mode volumes. An aerosol model with size distribution parameters and refractive index shown in Table 13 was found to be able to reconstruct the AERONET AOD with accuracy of order 0.01-0.02, if only the fine and coarse mode volumes are taken as input. This accuracy is similar to that of the AERONET AOD measurements themselves, and holds at most sites and wavelengths between 340 nm and 1020 nm. These parameters are therefore suggested for use in aerosol remote sensing algorithms to represent unpolluted marine aerosol.

Size distributions were found to have a dependence on the wind speed, with higher winds leading to an increased coarse mode total volume and volume mean radius. As the majority of the data were for wind speeds between 4 and 8 ms^{-1}, however, the global average coarse-mode radius can be used in most situations. The fine mode was comparatively unaffected. The AOD and Ångström exponent also showed an approximately linear relationship with wind speed. However, correlations were poor unless fits were performed to binned data, underlying the fact that wind speed alone is a poor predictor of the marine aerosol burden. When the relationship between wind speed and coarse mode aerosol volume was used to predict AOD observed on MAN cruises, the data were comparatively unbiased and had a scatter similar to the uncertainty on ship-measured AOD, although with a poor correlation, because of the small range of AOD. Relative humidity was also invesitaged, although poor sampling and potential for influence of either transported dust or cloud contamination for the lowest and highest humidities limit the strength of any conclusions which can be drawn. For the 88 % of the data within $60 \leq rh \leq 80$ % there was little change in size distribution parameters. Similarly, SST and columnar water vapor were not found to have a strong impact on aerosol size distribution parameters, within the ranges sampled.

Lidar ratios calculated from the results in this work give results approximately 50 % higher than those used for operational CALIOP algorithm at 532 nm, but more consistent with those from many other studies, consistent with an underestimate of marine AOD by CALIOP as observed in other studies.

Acknowledgements

This work was supported by a grant from the NASA MEaSUREs program, managed by M. Maiden. The AERONET (C. McClain, R. Frouin, J. Sciare, M. A. Lander, R. Wagener) and MAN (S. Piketh, R. Losno, P. Croot, J. Sciare, N. Nelson) PIs are thanked for the creation and maintenance of the Sun-photometer datasets. The Alfred Wegener Institute for Polar and Marine Research is thanked for the meteorological data from RV Polarstern. NCEP data were obtained from the SeaWiFS Ocean Biology Processing Group data distribution service. The authors thank A. Sinyuk for assistance in verification of the results of Mie computations.

Appendix A: Relation between number and volume size distributions

For individual lognormal components, the relationships between the volume and number distribution parameters may be calculated using Equations 2 and 6 by first noting that (dropping subscripted i)

$$\begin{aligned}\frac{dV(r)}{d\ln(r)} &= \frac{4\pi r^3}{3}\frac{C_n}{\sqrt{2\pi}\sigma}e^{-\frac{1}{2}\left(\frac{\ln(r)-\ln(r_n)}{\sigma}\right)^2} \\ &= \frac{4\pi}{3}\frac{C_n}{\sqrt{2\pi}\sigma}e^{-\frac{1}{2}\left(\frac{\ln(r)-\ln(r_n)}{\sigma}\right)^2+3\ln(r)} \qquad \text{(A1)}\end{aligned}$$

then expanding the exponential term

$$\begin{aligned}&-\frac{1}{2}\left(\frac{\ln(r)-\ln(r_n)}{\sigma}\right)^2+3\ln(r) \\ &= -\frac{1}{2\sigma^2}\left[\ln^2(r)-2\ln(r_n)\ln(r)+\ln^2(r_n)-6\sigma^2\ln(r)\right] \qquad \text{(A2)}\end{aligned}$$

multiplying Equation A1 by

$$1 = e^{3\ln(r_n)+4.5\sigma^2}e^{-3\ln(r_n)-4.5\sigma^2} \qquad \text{(A3)}$$

and combining the second exponential factor in Equation A3 with Equation A2 to give

$$\begin{aligned}-\frac{1}{2\sigma^2}[\ln^2(r) &- 2\ln(r_n)\ln(r)+\ln^2(r_n) \\ &- 6\sigma^2\ln(r)+6\sigma^2\ln(r_n)+9\sigma^4], \qquad \text{(A4)}\end{aligned}$$

which simplifies to

$$-\frac{1}{2}\left(\frac{\ln(r)-[\ln(r_n)+3\sigma^2]}{\sigma}\right)^2. \qquad \text{(A5)}$$

From this the definition

$$\ln(r_v) = \ln(r_n)+3\sigma^2 \qquad \text{(A6)}$$

leads to the result that

Hasekamp, O. P., and J. Landgraf (2007), Retrieval of aerosol properties over land surfaces: capabilities of multi-viewing-angle intensity and polarization measurements, *Appl. Opt.*, *46*(16), 3332–3344, doi:10.1364/AO.46.003332.

Hegg, D. A., J. Livingston, P. V. Hobbs, T. Novakov, and P. Russell (1997), Chemical apportionment of aerosol column optical depth off the mid-Atlantic coast of the Unites States, *J. Geophys. Res.*, *102*(D21), 25,293–25,303, doi:10.1029/97JD02293.

Henderson, B. G., P. Chylek, W. M. Porch, and M. K. Dubey (2006), Satellite remote sensing of aerosols generated by the Island of Nauru, *J. Geophys. Res.*, *111*(D22209), doi:10.1029/2005JD006850.

Hess, M., P. Koepke, and I. Schult (1998), Optical properties of aerosols and clouds: The software package OPAC, *Bull. Am. Met. Soc.*, *79*(5), 831–944, doi:10.1175/1520-0477(1998)079.

Hinds, W. C. (1999), *Aerosol technology: properties, behavior, and measurement of airborne particles*, second ed., 75–110 pp., Wiley Interscience, New York, Chichester, Weinheim, Brisbane, Singapore, and Toronto.

Holben, B. N., T. F. Eck, I. Slutsker, D. Tanré, J. P. Buis, A. Setzer, E. Vermote, J. A. Reagan, Y. J. Kaufman, T. Nakajima, F. Lavenu, I. Jankowiak, and A. Smirnov (1998), AERONET: A federated instrument network and data archive for aerosol characterization, *Remote Sens. Environ.*, *66*, 1–16, doi:10.1016/S0034-4257(98)00031-5.

Holben, B. N., D. Tanré, A. Smirnov, T. F. Eck, I. Slutsker, N. Abuhassan, W. W. Newcomb, J. S. Schafer, B. Chatenet, F. Lavenu, Y. J. Kaufman, J. Vande Castle, A. Setzer, B. Markham, D. Clark, R. Frouin, R. Halthore, A. Karneli, N. T. O'Neill, C. Pietras, R. T. Pinker, K. Voss, and G. Zibordi (2001), An emerging ground-based aerosol climatology: Aerosol optical depth from AERONET, *J. Geophys. Res.*, *106*(D11), 12,067–12,097, doi:10.1029/2001JD900014.

Holben, B. N., E. T. F., I. Slustker, A. Smirnov, A. Sinyuk, J. Shafer, D. Giles, and O. Dubocik (2006), AERONET's version 2.0 quality assurance criteria, in *Proceedings of SPIE, volume 6408*, paper number 6408-27.

Hoppel, W. A., J. W. Fitzgerald, G. M. Frick, and R. E. Larson (1990), Aerosol size distributions and optical properties found in the marine boundary layer over the Atlantic Ocean, *J. Geophys. Res.*, *95*(D4), 3659–3686.

Huang, H., G. E. Thomas, and R. G. Grainger (2010), Relationship between wind speed and aerosol optical depth over remote ocean, *Atmos. Chem. Phys.*, *10*, 5943–5950, doi:10.5194/acp-10-5943-2010.

Irshad, R., R. G. Grainger, D. M. Peters, R. A. McPheat, K. M. Smith, and G. E. Thomas (2009), Laboratory measurements of the optical properties of sea salt aerosol, *Atmos. Chem. Phys.*, *9*, 221–230, doi:10.5194/acp-9-221-2009.

Jaeglé, L., P. K. Quinn, T. S. Bates, B. Alexander, and J.-T. Lin (2011), Global distribution of sea salt aerosols: new constraints from in situ and remote sensing observations, *Atmos. Chem. Phys.*, *11*, 3137–3157, doi:10.5194/acp-11-3137-2011.

Kaufman, Y. J., A. Smirnov, B. N. Holben, and O. Dubovik (2001), Baseline maritime aerosol: Methodology to derive the optical thickness and scattering properties, *Geophys. Res. Lett.*, *28*(17), 3251–3254, doi:10.1029/2001GL013312.

Kiliyanpilakkil, V. P., and N. Meskhidze (2011), Deriving the effect of wind speed on clean maritime aerosol optical properties using the A-Train satellites, *Atmos. Chem. Phys. Discuss.*, *11*, 4599–4630, doi:10.5194/acpd-11-4599-2011.

Knobelspiesse, K. D., C. Pietras, G. S. Fargion, M. Wang, R. Frouin, M. A. Miller, A. Subramaniam, and W. M. Balch (2004), Maritime aerosol optical thickness measured by handheld Sun photometers, *Remote Sens. Environ.*, *93*(1–2), 87–106, doi:10.1016/j.rse.2004.06.018.

Kokhanovsky, A. A., J. L. Deuzé, D. J. Diner, O. Dubovik, F. Ducos, C. Emde, M. J. Garay, R. G. Grainger, A. Heckel, M. Herman, I. L. Katsev, J. Keller, R. Levy, P. R. J. North, A. S. Prikhach, V. V. Rozanov, A. M. Sayer, Y. Ota, D. Tanré, G. E. Thomas, and E. P. Zege (2010), The determination of spectral aerosol optical thickness from satellites: an intercomparison of algorithms using synthetic backscattered solar light characteristics, *Atmos. Meas. Tech.*, *3*, 909–932, doi:10.5194/amt-3-909-2010.

König-Langlo, G. (2005a), Continuous meteorological surface measurement during POLARSTERN cruise ANT-XX/1, doi:10.1594/PANGAEA.326651, Alfred Wegener Institute for Polar and Marine Research, Bremerhaven.

König-Langlo, G. (2005b), Continuous meteorological surface measurement during POLARSTERN cruise ANT-XXI/5, doi:10.1594/PANGAEA.326649, Alfred Wegener Institute for Polar and Marine Research, Bremerhaven.

König-Langlo, G. (2005c), Continuous meteorological surface measurement during POLARSTERN cruise ANT-XXII/5, doi:10.1594/PANGAEA.326644, Alfred Wegener Institute for Polar and Marine Research, Bremerhaven.

König-Langlo, G. (2005d), Continuous meteorological surface measurement during POLARSTERN cruise ANT-XX/3, doi:10.1594/PANGAEA.326653, Alfred Wegener Institute for Polar and Marine Research, Bremerhaven.

König-Langlo, G. (2006), Continuous meteorological surface measurement during POLARSTERN cruise ANT-XXIII/1, doi:10.1594/PANGAEA.544834, Alfred Wegener Institute for Polar and Marine Research, Bremerhaven.

König-Langlo, G. (2008a), Continuous meteorological surface measurement during POLARSTERN cruise ANT-XXIV/1, doi:10.1594/PANGAEA.692897, Alfred Wegener Institute for Polar and Marine Research, Bremerhaven.

König-Langlo, G. (2008b), Continuous meteorological surface measurement during POLARSTERN cruise ANT-XXIII/10, doi:10.1594/PANGAEA.692892, Alfred Wegener Institute for Polar and Marine Research, Bremerhaven.

König-Langlo, G. (2008c), Continuous meteorological surface measurement during POLARSTERN cruise ANT-XXIV/4, doi:10.1594/PANGAEA.708847, Alfred Wegener Institute for Polar and Marine Research, Bremerhaven.

König-Langlo, G. (2009a), Continuous meteorological surface measurement during POLARSTERN cruise ANT-XXV/1, doi:10.1594/PANGAEA.716915, Alfred Wegener Institute for Polar and Marine Research, Bremerhaven.

König-Langlo, G. (2009b), Continuous meteorological surface measurement during POLARSTERN cruise ANT-XXV/5, doi:10.1594/PANGAEA.717127, Alfred Wegener Institute for Polar and Marine Research, Bremerhaven.

König-Langlo, G. (2010a), Continuous meteorological surface measurement during POLARSTERN cruise ANT-XXVI/1, doi:doi:10.1594/PANGAEA.743573, Alfred Wegener Institute for Polar and Marine Research, Bremerhaven.

König-Langlo, G. (2010b), Continuous meteorological surface measurement during POLARSTERN cruise ANT-XXVI/4, doi:10.1594/PANGAEA.743577, Alfred Wegener Institute for Polar and Marine Research, Bremerhaven.

Kotchenruther, R. A., P. V. Hobbs, and D. A. Hegg (1999), Humidification factors for atmospheric aerosols off the mid-Atlantic coast of the United States, *J. Geophys. Res.*, *104*(D2), 2239–2251.

Lehahn, Y., I. Koren, E. Boss, Y. Ben-Ami, and O. Altaratz (2010), Estimating the maritime component of aerosol optical depth and its dependency on surface wind speed using satellite data, *Atmos. Chem. Phys.*, *10*, 6711–6720, doi:10.5194/acp-10-6711-2010.

Lewis, E. R., and S. E. Schwartz (2004), *Sea Salt Aerosol Production: Mechanisms, Methods, Measurements, and Models*, 9–100; 119–182; 256–273 pp., American Geophysical Union, Washington, geophysical monograph series, volume 152, AGU code GM1524173.

Lobert, J. M., and J. M. Harris (2002), Trace gases and air mass origin at Kaashidhoo, Indian Ocean, *J. Geophys. Res.*, *107*(8013), doi:10.1029/2001JD000731.

Lovett, R. F. (1978), Quantitative measurement of airborne sea-salt in the North Atlantic, *Tellus*, *30*, 358–364, doi:10.1111/j.2153-3490.1978.tb00851.x.

Magi, B. I., P. V. Hobbs, T. W. Kirchstetter, T. Novakov, D. A. Hegg, S. Gao, J. Redemann, and B. Schmid (2005), Aerosol properties and chemical apportionment of aerosol optical depth at locations off the U. S. East Coast in July and August 2001, *J. Atmos. Sci.*, *62*(4), 919–933, doi:10.1175/JAS3263.1.

Mishchenko, M. I., L. D. Travis, R. A. Kahn, and R. A. West (1997), Modeling phase functions for dustlike tropospheric aerosols using a shape mixture of randomly oriented polydisperse spheroids, *J. Geophys. Res.*, *102*(D14), 16,831–16,847, doi:10.1029/96JD02110.

Monahan, E. C., C. W. Fairall, K. L. Davidson, and P. J. Boyle (1983), Observed inter-relations between 10m winds, ocean whitecaps and marine aerosols, *Quart. J. Royal Met. Soc.*, *109*(460), 379–392, doi:10.1002/qj.49710946010.

$$r_{\mathrm{v}} = r_{\mathrm{n}} e^{3\sigma^2}, \tag{A7}$$

and, returning to Equation A1 with the remaining first exponential factor from Equation A3,

$$\begin{aligned}\frac{dV(r)}{d\ln(r)} &= \frac{4\pi}{3}\frac{C_{\mathrm{n}}}{\sqrt{2\pi}\sigma} e^{3\ln(r_{\mathrm{n}}) + 4.5\sigma^2} e^{-\frac{1}{2}\left(\frac{\ln(r)-\ln(r_{\mathrm{v}})}{\sigma}\right)^2} \\ &= \frac{4\pi}{3} r_{\mathrm{n}}^3 e^{4.5\sigma^2} \frac{C_{\mathrm{n}}}{\sqrt{2\pi}\sigma} e^{-\frac{1}{2}\left(\frac{\ln(r)-\ln(r_{\mathrm{v}})}{\sigma}\right)^2}, \end{aligned} \tag{A8}$$

hence

$$C_{\mathrm{v}} = \frac{4\pi}{3} {r_{\mathrm{n}}}^3 e^{4.5\sigma^2} C_{\mathrm{n}}. \tag{A9}$$

References

Ångström, A. (1929), On the atmospheric transmission of Sun radiation and on dust in the air, *Geogr. Ann.*, *12*, 130–159.

Ackermann, J. (1998), The extinction-to-backscatter ratio of tropospheric aerosol: A numerical study, *J. Atmos. Oceanic Technol.*, *15*, 1043.

Adames, A. F., M. Reynolds, A. Smirnov, D. S. Covert, and T. P. Ackerman (2011), Comparison of MODIS ocean aerosol retrievals with ship-based Sun photometer measurements from the Around the Americas expedition, *J. Geophys. Res.*, in press.

Ahmad, Z., B. A. Franz, C. R. McClain, E. J. Kwiatowska, J. Werdell, E. P. Shettle, and B. N. Holben (2010), New aerosol models for the retrieval of aerosol optical thickness and normalized water-leaving radiances from the SeaWiFS and MODIS sensors over coastal regions and open oceans, *Appl. Opt.*, *49*(29), 5545–5560, doi:10.1364/AO.49.005545.

Alexandrov, M. D., B. Schmid, D. D. Turner, B. Cairns, V. Oinas, A. A. Lacis, S. I. Gutman, E. R. Westwater, A. Smirnov, and J. Eilers (2009), Columnar water vapor retrievals from multifilter rotating shadowband radiometer data, *J. Geophys. Res.*, *114*(D02306), doi:10.1029/2008JD010543.

Anguelova, M., and F. Webster (2006), Whitecap coverage from satellite measurements: A first step toward modeling the variability of ocean whitecaps, *J. Geophys. Res.*, *111*, doi:10.1029/2005JC003158.

Ayers, G. P. (2001), Comment on regression analysis of air quality data, *Atmos. Env.*, *35*, 2423–2425, doi:10.1016/S1352-2310(00)00527-6.

Blanchard, D. C., and A. H. Woodcock (1980), *The production, concentration, and vertical distribution of the sea-salt aerosol*, 330–347 pp., Wiley, doi:10.1111/j.1749-6632.1980.tb17130.x, in: Annals of the New York Academy of Sciences, Volume 338, Aerosols: Anthropogenic and Natural, Sources and Transport.

Bloomfield, P., and W. Steiger (1980), Least absolute deviations curve-fitting, *SIAM J. Sci. and Stat. Comput.*, *1*(2), 290–301, doi:10.1137/0901019.

Cattrall, C., J. Reagan, K. Thome, and O. Dubovik (2005), Variability of aerosol and spectral lidar and backscatter and extinction ratios of key aerosol types derived from selected Aerosol Robotic Network locations, *J. Geophys. Res.*, *110*(D10S11).

Clarke, A. D., S. R. Owens, and J. Zhou (2006), An ultrafine sea-salt flux from breaking waves: Implicatioms for cloud condensation nuclei in the remote marine atmosphere, *J. Geophys. Res.*, *111*(D06202), doi:10.1029/2005JD006565.

Derber, J. C., D. F. Parrish, and S. Lord (1991), The new global operational analysis system at the National Meteorological Center, *Wea. Forecasting*, *6*, 538–547, www.emc.ncep.noaa.gov/gmb/gdas/index.html.

Dubovik, O., and M. D. King (2000), A flexible inversion algorithm for retrieval of aerosol optical properties from Sun and sky radiance measurements, *J. Geophys. Res.*, *105*(D16), 20,673–20,696.

Dubovik, O., A. Smirnov, B. N. Holben, M. D. King, Y. J. Kaufman, T. F. Eck, and I. Slutsker (2000), Accuracy assessments of aerosol optical properties retrieved from aerosol robotic network (AERONET) Sun and sky radiance measurements, *J. Geophys. Res.*, *105*(D8), 9791–9806.

Dubovik, O., B. Holben, T. F. Eck, A. Smirnov, Y. Kaufman, M. King, D. Tanré, and I. Slutsker (2002), Variability and optical properties of key aerosol types observed in worldwide locations, *J. Atm. Sci.*, *59*, 590–608, doi:10.1175/1520-0469(2002)059<0590:VOAAOP>2.0.CO;2.

Dubovik, O., A. Sinyuk, T. Lapyonok, B. Holben, M. Mischenko, P. Yang, T. Eck, H. Volten, O. Muñoz, B. Veihelmann, W. J. van der Zande, J.-F. Leon, M. Sorokin, and I. Slutsker (2006), The application of spheroid models to account for aerosol particle non-sphericity in remote sensing of desert dust, *J. Geophys. Res.*, *111*(D11208), doi:10.1029/2005JD006619.

Dubovik, O., M. Herman, A. Holdak, T. Lapyonok, D. Tanré, J. L. Deuzé, F. Ducos, A. Sinyuk, and A. Lopatin (2011), Stastically optimized inversion algorithm for enhanced retrieval of aerosol properties from spectral multi-angle polarimetric satellite observations, *Atmos. Meas. Tech.*, *4*, 975–1018, doi:10.5194/amt-4-975-2011.

Eck, T. F., B. N. Holben, J. S. Reid, O. Dubovik, A. Smirnov, N. T. O'Neill, I. Slutsker, and S. Kinne (1999), Wavelength dependence of the optical depth of biomass burning, urban, and desert dust aerosols, *J. Geophys. Res.*, *104*(D24), 31,333–31,349.

Eck, T. F., B. N. Holben, O. Dubovik, A. Smirnov, P. Goloub, H. B. Chen, B. Chatenet, L. Gomes, X.-Y. Zhang, S.-C. Tsay, Q. Ji, D. Giles, and I. Slutsker (2005), Columnar aerosol optical properties at AERONET sites in central eastern Asia and aerosol transport to the tropical mid-Pacific, *J. Geophys. Res.*, *110*(D06202), doi:10.1029/2004JD005274.

Exton, H. J., J. Latham, P. M. Park, S. J. Perry, M. H. Smith, and R. R. Allan (1985), The production and dispersal of marine aerosol, *Quart. J. Royal Met. Soc.*, *111*(469), 817–837, doi:10.1002/qj.49711146909.

Fraser, R. S., S. Mattoo, E.-N. Yeh, and C. R. McClain (1997), Algorithm for atmospheric and glint corrections of satellite measurements of ocean pigment, *J. Geophys. Res.*, *102*(D14), 17,107–17,118, doi:10.1029/97JD00357.

Fuentes, E., H. Coe, D. Green, G. de Leeuw, and G. McFiggans (2010), On the impacts of phytoplankton-derived organic matter on the properties of the primary marine aerosol Part 1: Source fluxes, *Atmos. Chem. Phys.*, *10*, 9295–9317, doi:10.5194/acp-10-9295-2010.

Galanter, M., H. Levy II, and G. R. Carmichael (2000), Impacts of biomass burning on tropospheric CO, NO_x , and O_3, *J. Geophys. Res.*, *105*(D5), doi:10.1029/1999JD901113.

Gathman, S. G. (1983), Optical properties of the marine aerosol as predicted by the Navy aerosol model, *Opt. Eng*, *22*, 57–62.

Glantz, P., E. D. Nilsson, and W. von Hoyningen-Huene (2009), Estimating a relationship between aerosol optical thickness and surface wind speed over the ocean, *Atmos. Res.*, *92*, 56–68, doi:10.1016/j.atmosres.2008.08.010.

Gong, S. L. (2003), A paramterization of sea-salt aerosol source function for sub- and super-micron particles, *Global Biogeochem. Cycles*, *17*(1097), doi:10.1029/2003GB002079.

Grandey, B. S., P. Stier, T. M. Wagner, R. G. Grainger, and K. I. Hodges (2011), The effect of extratropical cyclones on satellite-retrieved aerosol properties over ocean, *Geophys. Res. Lett.*, *38*(L13805), doi:10.1029/2011GL047703.

Hänel, G. (1976), The properties of atmospheric aerosol particles as functions of the relative humidity at thermodynamic equilibrium with the surrounding moist air, *Adv. Geophys.*, *19*, 73–1988, doi:10.1016/S0065-2687(08)60142-9.

Hansen, J. E., and L. D. Travis (1974), Light scattering in planetary atmospheres, *Space Sci. Rev.*, *16*(4), 527–610, doi:10.1007/BF00168069.

Hasekamp, O., P. Litvinov, and A. Butz (2011), Aerosol properties over the ocean from PARASOL multi-angle photopolarimetric measurements, *J. Geophys. Res.*, doi:10.1029/2010JD015469, in press.

Mulcahy, J. P., C. D. O'Dowd, S. G. Jennings, and D. Ceburnis (2008), Significant enhancement of aerosol optical depth in marine air under high wind conditions, *J. Geophys. Res.*, *35*(L16819), doi:10.1029/2008GL034303.

Müller, D., A. Ansmann, I. Mattis, M. Tesche, U. Wandinger, D. Althausen, and G. Pisani (2007), Aerosol-type-dependent lidar ratios observed with Raman lidar, *J. Geophys. Res.*, *112*(D16202), doi:10.1029/2006JD008292.

Murray, M. J., M. R. Allen, C. J. Merchant, A. R. Harris, and C. J. Donlon (2000), Direct observations of skin-bulk SST variability, *Geophys. Res. Lett.*, *27*(8), 1171–1174, doi: 10.1029/1999GL011133.

O'Dowd, C. D., and G. de Leeuw (2007), Marine aerosol production: a review of the current knowledge, *Phil. Trans. R. Soc. A*, *365*, doi:10.1098/rsta.2007.2043.

Omar, A. H., D. M. Winker, M. A. Vaughan, Y. Hu, C. A. Trepte, R. A. Ferrare, K.-P. Lee, and C. A. Hostetler (2009), The CALIPSO automated aerosol classification and lidar ratio selection algorithm, *J. Atmos. Oceanic Technol.*, *26*, 1994–2014, doi:10.1175/2009JTECHA1231.1.

O'Neill, N., T. Eck, A. Smirnov, B. Holben, and S. Thulasiraman (2006), Spectral deconvolution algorithm technical memo, *Tech. rep.*, NASA Goddard Space Flight Center, revision April 26, 2006, version 4, available online from http://aeronet.gsfc.nasa.gov/new_web/PDF/tauf_tauc_technical_memo1.pdf [Accessed December 2010].

O'Neill, N. T., T. F. Eck, A. Smirnov, B. N. Holben, and S. Thulasiraman (2003), Spectral discrimination of coarse and fine mode optical depth, *J. Geophys. Res.*, *108*(D17), 4559–4573, doi:10.1029/2002JD002975.

Oo, M., and R. Holz (2011), Improving the CALIOP aerosol optical depth using combined MODIS-CALIOP observations and CALIOP integrated attenuated total color ratio, *J. Geophys. Res.*, *116*(D14201), doi:10.1029/2010JD014894.

Pant, V., C. G. Deshpande, and A. A. Kamra (2008), On the aerosol number concentration-wind speed relationship during a severe cyclonic storm over south Indian Ocean, *J. Geophys. Res.*, *113*(C02206), doi:10.1029/2006JD008035.

Pedrós, R., V. Estellés, M. Sicard, J. L. Gómez-Amo, M. P. Utrillas, J. A. Martínez-Lozano, F. Rocadenbosch, C. Pérez, and J. M. B. Recio (2010), Climatology of the aerosol extinction-to-backscatter ratio from Sun-photometric measurements, *IEEE Trans. Geosci. Remote Sens.*, *48*(1), 237–249, doi:10.1109/TGRS.2009.2027699.

Reid, J. S., B. Brooks, K. K. Crahan, D. A. Hegg, T. F. Eck, N. O'Neill, G. de Leeuw, E. A. Reid, and K. D. Anderson (2006), Reconciliation of coarse mode sea-salt aerosol particle size measurements and parameterizations at a subtropical ocean receptor site, *J. Geophys. Res.*, *111*(D02202), doi: 10.1029/2005JD006200.

Remer, L. A., D. Tanré, and Y. J. Kaufman (2006), Algorithm for remote sensing of tropospheric aerosol from MODIS: Collection 5, *Tech. rep.*, NASA Goddard Space Flight Center, ATBD-MOD-02, product ID MOD04/MYD04, available online from http://modis.gsfc.nasa.gov/data/atbd/ [Accessed December 2010].

Reynolds, R. W., T. M. Smith, C. Liu, D. B. Chelton, K. S. Casey, and M. G. Schlax (2006), Daily high-resolution blended analyses for sea surface temperature, *J. Climate*, *20*, 5473–5496, doi:10.1175/2007JCLI1824.1.

Sakerin, S. M., D. M. Kabanov, A. V. Smirnov, and B. N. Holben (2008), Aerosol optical depth of the atmosphere over the ocean in the wavelength range 0.37-4 μm, *Int. J. Remote Sens.*, *29*(9), 2519–2547, doi:10.1080/01431160701767492.

Satheesh, S. K., J. Srinivasan, and K. Krishna Moorthy (2006), Contribution of sea-salt to aerosol optical depth over the Arabian Sea derived from MODIS observations, *Geophys. Res. Lett.*, *33*(L03809), doi:10.1029/2005GL024856.

Sayer, A. M., G. E. Thomas, and R. G. Grainger (2010), A sea surface reflectance model for (A)ATSR, and application to aerosol retrievals, *Atmos. Meas. Tech.*, *3*, 813–838, doi: 10.5194/amt-3-813-2010.

Sayer, A. M., N. C. Hsu, C. Bettenhausen, Z. Ahmad, B. N. Holben, A. Smirnov, G. E. Thomas, and J. Zhang (2011), SeaWiFS ocean aerosol retrieval (SOAR): algorithm, validation, and comparison with other datasets, *J. Geophys. Res.*, submitted.

Sellegri, K., C. D. O'Dowd, Y. J. Yoon, S. G. Jennings, and G. de Leeuw (2006), Surfactants and submicron sea spray generation, *J. Geophys. Res.*, *111*(D22215), doi: 10.1029/2005JD006658.

Shettle, E. P., and R. W. Fenn (1979), Models for the aerosols of the lower atmosphere and the effects of humidity variations on their optical properties, *Tech. rep.*, Air force geophysics laboratory, report number AFGL-TR-79-0214, environmental research paper 676.

Silva, A. M., M. L. Bugalho, M. J. Costa, W. von Hoyningen-Huene, T. Schmidt, J. Heintzenberg, and S. Henning (2002), Aerosol optical properties from columnar data during the second Aerosol Characterization Experiment on the south coast of Portugal, *J. Geophys. Res.*, *107*(D22, 4642), doi: 10.1029/2002JD002196.

Smirnov, A., Y. Villevalde, N. T. O'Neill, A. Royer, and A. Tarussov (1995), Aerosol optical depth over the oceans: analysis in terms of synoptic air mass types, *J. Geophys. Res.*, *100*(D8), 16,639–16,650.

Smirnov, A., B. N. Holben, T. F. Eck, O. Dubovik, and I. Slutsker (2000a), Cloud-screening and quality control algorithms for the AERONET database, *Remote Sens. Environ.*, *73*(3), 337–349.

Smirnov, A., B. N. Holben, D. Savoie, J. M. Prospero, Y. J. Kaufman, D. Tanr'e, T. F. Eck, and I. Slutsker (2000b), Relationship between column aerosol optical thickness and in situ ground based dust concentrations over Barbados, *Geophys. Res. Lett.*, *27*(11), 1643–1646, doi:10.1029/1999GL011336.

Smirnov, A., B. N. Holben, O. Dubovik, N. T. O'Neill, L. A. Remer, T. F. Eck, I. Slutsker, and D. Savoie (2000c), Measurement of atmospheric optical properties on U.S. Atlantic coast sites, ships, and Bermuda during TARFOX, *J. Geophys. Res.*, *105*(D8), 9887–9901, doi:10.1029/1999JD901067.

Smirnov, A., B. N. Holben, Y. J. Kaufman, O. Dubovik, T. F. Eck, I. Slutsker, C. Pietras, and R. H. Halthore (2002), Optical properties of atmospheric aerosol in maritime environments, *J. Atmos. Sci.*, *59*, 501–523.

Smirnov, A., B. N. Holben, O. Dubovik, R. Frouin, T. F. Eck, and I. Slutsker (2003a), Maritime component in aerosol optical models derived from Aerosol Robotic Network data, *J. Geophys. Res.*, *108*(D1), doi:10.1029/2002JD002701.

Smirnov, A., B. N. Holben, T. F. Eck, O. Dubovik, and I. Slutsker (2003b), Effect of wind speed on columnar aerosol optical properties at Midway Island, *J. Geophys. Res.*, *108*(D24), doi: 10.1029/2003JD003879.

Smirnov, A., B. N. Holben, A. Lyapustin, I. Slutsker, and T. F. Eck (2004), AERONET processing algorithms refinement, in *AERONET Workshop, El Arenosillo, Spain*.

Smirnov, A., B. N. Holben, I. Slutsker, D. M. Giles, C. R. McClain, T. F. Eck, S. M. Sakerin, A. Macke, P. Croot, G. Zibordi, P. K. Quinn, J. Sciare, S. Kinne, M. Harvey, T. J. Smyth, S. Piketh, T. Zielinski, A. Proshuninsky, J. I. Goes, N. B. Nelson, P. Larouche, V. F. Radionov, P. Goloub, K. K. Moorthy, R. Matarresse, E. J. Robertson, and F. Jourdin (2009), Maritime aerosol network as a component of aerosol robotic network, *J. Geophys. Res.*, *112*(D06204), doi: 10.1029/2008JD011257.

Smirnov, A., B. N. Holben, D. M. Giles, I. Slutsker, N. T. O'Neill, T. F. Eck, A. Macke, P. Croot, Y. Courcoux, S. M. Sakerin, T. J. Smyth, T. Zielinski, G. Zibordi, J. I. Goes, M. J. Harvey, P. K. Quinn, N. B. Nelson, V. F. Radionov, C. M. Duarte, R. Losno, J. Sciare, K. J. Voss, S. Kinne, N. R. Nalli, E. Joseph, K. Krishna Moorthy, D. S. Covert, S. K. Gulev, G. Milinevsky, P. Larouche, S. Belanger, E. Horne, M. Chin, L. A. Remer, R. A. Kahn, J. S. Reid, M. Schulz, C. L. Heald, J. Zhang, K. Lapina, R. G. Kleidman, J. Griesfeller, B. J. Gaitley, Q. Tan, and T. L. Diehl (2011), Maritime Aerosol Network as a component of AERONET-first results and comparison with global aerosol models and satellite retrievals, *Atmos. Meas. Tech.*, *4*, 583–597, doi:10.5194/amt-4-583-2011.

Smirnov, A. V., and K. S. Shifrin (1989), Relationship of optical thickness to humidity of air above the ocean, *Izv. Atmos. Ocean. Phys.*, *25*(5), 374–379, english translation.

Wagner, F., and A. M. Silva (2008), Some considerations about Ångström exponent distributions, *Atmos. Chem Phys.*, *8*, 481–489, doi:10.5194/acp-8-481-2008.

Wallcraft, A. J., A. B. Kara, C. N. Barron, E. J. Metzger, R. L. Pauley, and M. A. Bourassa (2009), Comparisons of monthly mean 10 m wind speeds from satellites and NWP products over the global ocean, *J. Geophys. Res.*, *114*(D16109), doi: 10.1029/2008JD011696.

Zieliński, T., and A. Zieliński (2002), Aerosol extinction and aerosol optical thickness in the atmosphere over the Baltic Sea determined with lidar, *J. Aerosol Sci.*, *33*(6), 907–921, doi:10.1016/S0021-8502(02)00043-5.

B. N. Holben, Biospheric Sciences Branch, NASA Goddard Space Flight Center, Greenbelt, MD 20771, USA.

N. C. Hsu, Climate and Radiation Branch, NASA Goddard Space Flight Center, Greenbelt, MD 20771, USA.

A. M. Sayer, Climate and Radiation Branch, NASA Goddard Space Flight Center, Greenbelt, MD 20771, USA. (andrew.sayer@nasa.gov)

A. Smirnov, Biospheric Sciences Branch, NASA Goddard Space Flight Center, Greenbelt, MD 20771, USA.

Table 1. Locations of the AERONET sites used in this work, as well as the number and proportion of AERONET inversions passing the criteria for clean maritime conditions, as described in the text.

Site name	Latitude, degrees	Longitude, degrees	Elevation, m above sea level	Number of maritime	Proportion of maritime
Lanai	20.7350	-156.922	20	1113	0.79
Bermuda	32.3700	-64.6960	10	116	0.49
Kaashidhoo	4.96500	73.4660	0	50	0.20
Midway Island	28.2100	-177.378	20	484	0.86
Ascension Island	-7.97600	-14.4150	30	341	0.61
Tahiti	-17.5770	-149.606	98	375	0.82
Amsterdam Island	-37.8100	77.5730	30	32	0.68
Crozet Island	-46.4350	51.8500	221	8	0.47
Guam	13.4310	144.801	62	74	0.82
Nauru	-0.521000	166.916	7	101	0.91
Graciosa	39.0910	-28.0300	15	265	0.78

Table 2. Size distribution parameters for each site. The upper half of the table shows averaged (median) size distribution parameters for AERONET aerosol volume size distributions, and figures in parentheses indicate the SMAD (defined in the text). The lower half shows bimodal lognormal distribution parameters for fits to averaged AERONET aerosol volume size distributions, and figures in parentheses indicate one standard deviation uncertainty on the fit. Also shown for both cases are the mean values over all sites, and the mean weighted by the number of AERONET retrievals at each site.

Site name	$C_{v,f}$, $\mu m^3 \mu m^{-2}$	$C_{v,c}$, $\mu m^3 \mu m^{-2}$	$r_{v,f}$, μm	$r_{v,c}$, μm	σ_f	σ_c
AERONET average parameters						
Lanai	0.0050 (0.0030)	0.032 (0.013)	0.169 (0.019)	2.39 (0.25)	0.48 (0.037)	0.67 (0.040)
Bermuda	0.0080 (0.0044)	0.041 (0.024)	0.159 (0.024)	2.36 (0.51)	0.46 (0.036)	0.65 (0.047)
Kaashidhoo	0.0080 (0.0030)	0.037 (0.024)	0.182 (0.013)	2.35 (0.47)	0.45 (0.043)	0.71 (0.059)
Midway Island	0.0060 (0.0030)	0.044 (0.024)	0.167 (0.021)	2.41 (0.34)	0.47 (0.044)	0.66 (0.042)
Ascension Island	0.0090 (0.0044)	0.049 (0.019)	0.156 (0.015)	2.36 (0.32)	0.48 (0.053)	0.69 (0.033)
Tahiti	0.0040 (0.0015)	0.028 (0.013)	0.171 (0.021)	2.43 (0.33)	0.48 (0.034)	0.69 (0.033)
Amsterdam Island	0.0050 (0.0030)	0.028 (0.021)	0.183 (0.034)	2.30 (0.30)	0.52 (0.044)	0.70 (0.039)
Crozet Island	0.0030 (0.0030)	0.019 (0.022)	0.251 (0.065)	2.17 (0.31)	0.54 (0.099)	0.72 (0.077)
Guam	0.0060 (0.0030)	0.035 (0.019)	0.177 (0.031)	2.45 (0.29)	0.49 (0.031)	0.69 (0.034)
Nauru	0.0040 (0.0015)	0.031 (0.018)	0.181 (0.031)	2.55 (0.36)	0.49 (0.044)	0.67 (0.044)
Graciosa	0.0060 (0.0030)	0.030 (0.019)	0.173 (0.018)	2.34 (0.39)	0.52 (0.049)	0.74 (0.037)
Mean	0.0058	0.034	0.179	2.37	0.49	0.69
Weighted mean	0.0057	0.036	0.169	2.39	0.48	0.68
Bimodal fit to median distribution						
Lanai	0.0051 (0.0004)	0.031 (0.002)	0.156 (0.007)	2.55 (0.11)	0.50 (0.049)	0.72 (0.042)
Bermuda	0.0081 (0.0006)	0.041 (0.002)	0.145 (0.005)	2.54 (0.12)	0.46 (0.037)	0.73 (0.049)
Kaashidhoo	0.0078 (0.0005)	0.037 (0.002)	0.170 (0.005)	2.56 (0.13)	0.44 (0.032)	0.76 (0.052)
Midway Island	0.0056 (0.0004)	0.043 (0.002)	0.157 (0.006)	2.58 (0.10)	0.49 (0.043)	0.70 (0.039)
Ascension Island	0.0082 (0.0008)	0.047 (0.003)	0.139 (0.007)	2.56 (0.13)	0.45 (0.054)	0.73 (0.050)
Tahiti	0.0041 (0.0003)	0.027 (0.002)	0.161 (0.007)	2.72 (0.14)	0.51 (0.047)	0.69 (0.050)
Amsterdam Island	0.0037 (0.0002)	0.030 (0.002)	0.155 (0.004)	2.29 (0.15)	0.51 (0.030)	0.84 (0.066)
Crozet Island	0.0030 (0.0002)	0.022 (0.002)	0.190 (0.006)	2.54 (0.25)	0.49 (0.034)	0.94 (0.10)
Guam	0.0054 (0.0004)	0.034 (0.002)	0.170 (0.008)	2.62 (0.10)	0.56 (0.053)	0.74 (0.039)
Nauru	0.0035 (0.0003)	0.031 (0.002)	0.174 (0.009)	2.94 (0.14)	0.55 (0.056)	0.67 (0.049)
Graciosa	0.0062 (0.0005)	0.029 (0.002)	0.168 (0.008)	2.48 (0.16)	0.57 (0.052)	0.83 (0.068)
Mean	0.0055	0.034	0.162	2.58	0.50	0.76
Weighted Mean	0.0056	0.035	0.157	2.58	0.50	0.72

Table 3. Number of retrievals, AOD at two wavelengths, and Ångström exponent corresponding to AERONET aerosol volume size distributions, binned as a function of near-surface wind speed. Figures in parentheses indicate the SMAD.

Wind speed	Number of retrievals	τ_{440}	τ_{1020}	α
0-4 ms^{-1}	437	0.068 (0.022)	0.040 (0.013)	0.73 (0.14)
4-6 ms^{-1}	1022	0.065 (0.019)	0.039 (0.013)	0.60 (0.17)
6-8 ms^{-1}	1082	0.076 (0.025)	0.052 (0.018)	0.49 (0.18)
8-10 ms^{-1}	299	0.081 (0.025)	0.058 (0.020)	0.37 (0.15)
10+ ms^{-1}	67	0.090 (0.037)	0.062 (0.024)	0.34 (0.14)

Table 4. Size distribution parameters for average distributions binned as a function of near-surface wind speed. The upper half of the table shows averaged (median) size distribution parameters for AERONET aerosol volume size distributions, and figures in parentheses indicate the SMAD (defined in the text). The lower half shows bimodal lognormal distribution parameters for fits to averaged AERONET aerosol volume size distributions, and figures in parentheses indicate one standard deviation uncertainty on the fit.

Wind speed	$C_{v,f}$, $\mu m^3 \mu m^{-2}$	$C_{v,c}$, $\mu m^3 \mu m^{-2}$	$r_{v,f}$, μm	$r_{v,c}$, μm	σ_f	σ_c	$r_{eff,f}$, μm	$r_{eff,c}$, μm
AERONET average parameters								
0-4 ms^{-1}	0.0060 (0.0020)	0.024 (0.0090)	0.173 (0.013)	2.27 (0.25)	0.46 (0.027)	0.70 (0.041)	0.155 (0.012)	1.76 (0.18)
4-6 ms^{-1}	0.0060 (0.0020)	0.030 (0.0090)	0.168 (0.014)	2.38 (0.20)	0.48 (0.026)	0.69 (0.029)	0.150 (0.012)	1.87 (0.14)
6-8 ms^{-1}	0.0060 (0.0020)	0.040 (0.012)	0.167 (0.014)	2.43 (0.19)	0.49 (0.026)	0.68 (0.027)	0.148 (0.012)	1.90 (0.14)
8-10 ms^{-1}	0.0060 (0.0020)	0.051 (0.016)	0.168 (0.014)	2.45 (0.19)	0.50 (0.028)	0.68 (0.031)	0.149 (0.011)	1.92 (0.15)
10+ ms^{-1}	0.0050 (0.0020)	0.054 (0.021)	0.169 (0.020)	2.45 (0.28)	0.52 (0.018)	0.70 (0.040)	0.147 (0.016)	1.91 (0.18)
Bimodal fit to median distribution								
0-4 ms^{-1}	0.0059 (0.00034)	0.024 (0.0012)	0.167 (0.0054)	2.35 (0.11)	0.50 (0.035)	0.79 (0.047)	0.131 (0.0042)	1.58 (0.073)
4-6 ms^{-1}	0.0052 (0.00040)	0.030 (0.0016)	0.156 (0.0067)	2.56 (0.12)	0.49 (0.046)	0.73 (0.046)	0.122 (0.0052)	1.77 (0.080)
6-8 ms^{-1}	0.0055 (0.00050)	0.040 (0.0022)	0.152 (0.0079)	2.63 (0.12)	0.51 (0.056)	0.71 (0.046)	0.118 (0.0061)	1.84 (0.084)
8-10 ms^{-1}	0.0055 (0.00053)	0.048 (0.0028)	0.155 (0.0089)	2.72 (0.13)	0.53 (0.062)	0.69 (0.048)	0.119 (0.0068)	1.92 (0.091)
10+ ms^{-1}	0.0044 (0.00033)	0.049 (0.0030)	0.143 (0.0060)	2.70 (0.14)	0.50 (0.048)	0.76 (0.054)	0.111 (0.0047)	1.84 (0.099)

Table 5. Statistics of linear regression between wind speed and AOD or α (daily averages for both datasets) of the form τ (or α)$= a + b \times ws$, from direct-Sun and SDA AERONET data. Also shown is Pearson's linear correlation coefficient for the fit, R. The bottom row shows the fits when data from all sites are considered together.

Site	τ_{440}			τ_{1020}			$\tau_{f,500}$			$\tau_{c,500}$			α		
	a	b	R	a	b	R	a	b	R	a	b	R	a	b	R
Lanai	0.092	-0.0021	0.13	0.044	0.00058	0.053	0.082	-0.0015	0.10	0.042	-0.0021	0.23	0.79	-0.039	0.35
Bermuda	0.097	0.0028	0.20	0.053	0.0029	0.29	0.088	0.0026	0.20	0.046	-0.000021	0.0031	0.82	-0.024	0.31
Kaashidoo	0.12	0.0022	0.091	0.070	0.0033	0.18	0.11	0.0023	0.10	0.052	-0.0013	0.11	0.70	-0.036	0.27
Midway Island	0.069	0.0044	0.25	0.033	0.0051	0.37	0.063	0.0044	0.27	0.034	-0.00017	0.023	0.76	-0.039	0.40
Ascension Island	0.090	0.0053	0.13	0.047	0.0039	0.12	0.080	0.0052	0.14	0.039	0.00070	0.034	0.71	-0.024	0.11
Tahiti	0.082	0.00041	0.024	0.029	0.0011	0.058	0.075	0.00043	0.026	0.032	-0.00014	0.020	0.72	-0.021	0.17
Amsterdam Island	0.057	0.0030	0.30	0.033	0.0032	0.37	0.051	0.0030	0.32	0.016	0.0011	0.27	0.58	-0.013	0.17
Crozet Island	0.061	0.0015	0.12	0.044	0.0016	0.16	0.054	0.0017	0.14	0.021	0.00052	0.072	0.55	-0.011	0.13
Guam	0.097	0.000070	0.0029	0.051	0.0031	0.16	0.087	0.0011	0.048	0.051	-0.0023	0.17	0.90	-0.074	0.48
Nauru	0.055	0.0041	0.24	0.028	0.0047	0.23	0.052	0.0043	0.26	0.022	0.00055	0.087	0.60	-0.039	0.26
Graciosa	0.084	0.0051	0.31	0.047	0.0061	0.45	0.077	0.0053	0.34	0.044	-0.00049	0.074	0.75	-0.044	0.45
All sites	0.071	0.0036	0.20	0.033	0.0040	0.27	0.066	0.0034	0.21	0.031	0.00038	0.048	0.65	-0.022	0.21

Table 6. Number of retrievals, AOD at two wavelengths, Ångström exponent, and average wind speed corresponding to AERONET aerosol volume size distributions, binned as a function of near-surface relative humidity. Figures in parentheses indicate the SMAD.

Relative humidity	Number of retrievals	τ_{440}	τ_{1020}	α	Wind speed
0 - 50 %	4	0.10 (0.021)	0.082 (0.017)	0.22 (0.10)	5.07 ms^{-1}
50 - 60 %	67	0.081 (0.027)	0.058 (0.014)	0.35 (0.18)	6.42 ms^{-1}
60 - 65 %	270	0.068 (0.020)	0.044 (0.014)	0.49 (0.21)	6.53 ms^{-1}
65 - 70 %	718	0.068 (0.023)	0.044 (0.016)	0.49 (0.17)	6.77 ms^{-1}
70 - 75 %	920	0.074 (0.024)	0.045 (0.017)	0.59 (0.18)	6.13 ms^{-1}
75 - 80 %	647	0.074 (0.022)	0.046 (0.016)	0.60 (0.19)	5.53 ms^{-1}
80 - 85 %	237	0.069 (0.019)	0.044 (0.014)	0.66 (0.15)	5.10 ms^{-1}
85 - 90 %	38	0.060 (0.011)	0.050 (0.0098)	0.41 (0.14)	5.56 ms^{-1}
90 - 100 %	4	0.16 (0.0052)	0.14 (0.0068)	0.21 (0.021)	6.44 ms^{-1}

Table 7. As Table 4, except for AERONET distributions binned as a function of relative humidity.

Relative humidity	$C_{v,f}$, $\mu m^3 \mu m^{-2}$	$C_{v,c}$, $\mu m^3 \mu m^{-2}$	$r_{v,f}$, μm	$r_{v,c}$, μm	σ_f	σ_c	$r_{eff,f}$, μm	$r_{eff,c}$, μm
AERONET average parameters								
0 - 50 %	0.0050 (0.0010)	0.073 (0.0090)	0.186 (0.026)	2.49 (0.088)	0.53 (0.013)	0.64 (0.025)	0.162 (0.022)	1.99 (0.056)
50 - 60 %	0.0050 (0.0020)	0.051 (0.012)	0.169 (0.017)	2.51 (0.20)	0.49 (0.031)	0.68 (0.027)	0.150 (0.014)	1.98 (0.15)
60 - 65 %	0.0050 (0.0020)	0.035 (0.012)	0.173 (0.014)	2.40 (0.20)	0.49 (0.027)	0.67 (0.028)	0.154 (0.011)	1.90 (0.15)
65 - 70 %	0.0050 (0.0020)	0.036 (0.011)	0.168 (0.014)	2.46 (0.18)	0.49 (0.026)	0.68 (0.027)	0.149 (0.013)	1.93 (0.14)
70 - 75 %	0.0060 (0.0020)	0.035 (0.012)	0.166 (0.014)	2.38 (0.19)	0.48 (0.026)	0.69 (0.028)	0.149 (0.012)	1.87 (0.14)
75 - 80 %	0.0060 (0.0020)	0.033 (0.012)	0.168 (0.014)	2.33 (0.23)	0.48 (0.029)	0.69 (0.035)	0.150 (0.012)	1.82 (0.15)
80 - 85 %	0.0060 (0.0020)	0.031 (0.013)	0.171 (0.013)	2.37 (0.28)	0.47 (0.027)	0.69 (0.036)	0.152 (0.012)	1.84 (0.19)
85 - 90 %	0.0050 (0.0020)	0.032 (0.011)	0.174 (0.013)	2.21 (0.20)	0.54 (0.043)	0.72 (0.018)	0.152 (0.0090)	1.71 (0.15)
90 - 100 %	0.0080 (0.0010)	0.13 (0.023)	0.203 (0.032)	2.57 (0.24)	0.53 (0.00010)	0.74 (0.012)	0.175 (0.027)	1.96 (0.19)
Bimodal fit to median distribution								
0 - 50 %	0.0049 (0.00037)	0.070 (0.0050)	0.156 (0.0067)	2.89 (0.15)	0.51 (0.049)	0.62 (0.051)	0.121 (0.0052)	2.13 (0.11)
50 - 60 %	0.0050 (0.00047)	0.048 (0.0029)	0.159 (0.0091)	2.86 (0.14)	0.56 (0.064)	0.68 (0.048)	0.121 (0.0069)	2.03 (0.097)
60 - 65 %	0.0051 (0.00039)	0.035 (0.0019)	0.156 (0.015)	2.58 (0.12)	0.50 (0.027)	0.72 (0.045)	0.122 (0.012)	1.80 (0.081)
65 - 70 %	0.0049 (0.00046)	0.036 (0.0019)	0.153 (0.0083)	2.66 (0.11)	0.52 (0.059)	0.71 (0.043)	0.118 (0.0064)	1.86 (0.080)
70 - 75 %	0.0057 (0.00047)	0.034 (0.0019)	0.154 (0.0072)	2.59 (0.12)	0.50 (0.050)	0.72 (0.046)	0.120 (0.0056)	1.80 (0.082)
75 - 80 %	0.0058 (0.00044)	0.032 (0.0017)	0.156 (0.0065)	2.47 (0.11)	0.49 (0.045)	0.75 (0.045)	0.122 (0.0051)	1.70 (0.075)
80 - 85 %	0.0054 (0.00030)	0.030 (0.0017)	0.161 (0.0050)	2.55 (0.13)	0.49 (0.033)	0.77 (0.051)	0.126 (0.0039)	1.74 (0.087)
85 - 90 %	0.0043 (0.00042)	0.032 (0.0021)	0.155 (0.0093)	2.33 (0.14)	0.56 (0.067)	0.83 (0.064)	0.117 (0.0070)	1.53 (0.094)
90 - 100 %	0.0087 (0.00044)	0.13 (0.0099)	0.214 (0.0081)	2.68 (0.20)	0.67 (0.041)	0.87 (0.080)	0.153 (0.0058)	1.74 (0.13)

Table 8. Number of retrievals, AOD at two wavelengths, Ångström exponent, and average wind speed corresponding to AERONET aerosol volume size distributions, binned as a function of AERONET columnar water vapor. Figures in parentheses indicate the SMAD.

Water vapor	Number of retrievals	τ_{440}	τ_{1020}	α	Wind speed
0-1 cm	15	0.034 (0.019)	0.029 (0.020)	0.35 (0.15)	5.30 ms^{-1}
1-2 cm	508	0.077 (0.027)	0.052 (0.019)	0.46 (0.20)	6.44 ms^{-1}
2-2.5 cm	615	0.065 (0.021)	0.043 (0.015)	0.51 (0.18)	6.56 ms^{-1}
2.5-3 cm	713	0.070 (0.022)	0.044 (0.015)	0.60 (0.19)	6.00 ms^{-1}
3-3.5 cm	620	0.074 (0.021)	0.046 (0.016)	0.60 (0.18)	5.82 ms^{-1}
3.5-4 cm	291	0.071 (0.018)	0.046 (0.016)	0.62 (0.16)	5.91 ms^{-1}
4+ cm	143	0.071 (0.019)	0.043 (0.014)	0.63 (0.20)	5.27 ms^{-1}

Table 9. Refractive indices $m = n - ik$ for marine aerosol tested in this work, along with information on sources.

Case	Fine mode	Coarse mode	Note
1	1.37 - 0.001i	1.37 - 0.001i	*Smirnov et al.* [2003a]; average of AERONET inversion results for Lanai.
2	1.45 - 0.0035i	1.35 - 0.001i	*Remer et al.* [2006]; pair of oceanic components used in MODIS collection 5 aerosol retrieval.
3	1.39 - 0.003i	1.39 - 0.003i	*Silva et al.* [2002]; ground-based unpolluted maritime measurements on the Portuguese coast.
4	1.415 - 0.002i	$1.363 - 3 \times 10^{-9}$i	*Shettle and Fenn*, 1979/*Hess et al.*, 1998 at 500 nm and rh =70 %; fine: water soluble component; coarse: accumulation/coarse sea salt component.
5	1.415 - 0.002i	$1.434 - 3 \times 10^{-9}$i	As case 4, except real part of coarse mode from *Irshad et al.* [2009] infrared laboratory data at rh =74.2 %, retrieval value at 500 nm.

Table 10. Pearson's linear correlation coefficient (top portion), median (calculated - AERONET observed) bias (middle portion), and SMAD (bottom portion) between observed AERONET spectral AOD and Ångström exponent, and that calculated using the average 'lognormal fitted' fine and coarse-mode radii and spreads, for refractive index case 4 from Table 9.

Site	τ_{340}	τ_{380}	τ_{440}	τ_{500}	τ_{675}	τ_{870}	τ_{1020}	α
				Correlation coefficient				
Lanai	0.95	0.96	0.97	0.96	0.95	0.94	0.94	0.77
Bermuda	0.91	0.91	0.92	0.91	0.88	0.87	0.87	0.77
Kaashidhoo	0.89	0.90	0.91	0.90	0.89	0.89	0.88	0.88
Midway Island	0.90	0.91	0.92	0.92	0.92	0.93	0.94	0.88
Ascension Island	0.88	0.89	0.89	0.89	0.88	0.88	0.89	0.88
Tahiti	0.89	0.91	0.95	0.94	0.94	0.95	0.93	0.63
Amsterdam Island	0.95	0.95	0.96	0.96	0.96	0.96	0.97	0.74
Crozet Island	0.96	0.95	0.93	0.93	0.85	0.67	0.68	-0.97
Guam	0.84	0.84	0.84	0.84	0.83	0.79	0.78	0.76
Nauru	0.78	0.82	0.85	0.86	0.91	0.90	0.90	0.79
Graciosa	0.76	0.80	0.82	0.84	0.89	0.90	0.91	0.72
				Median bias				
Lanai	0.0015	0.0014	0.00067	-0.0026	-0.0015	-0.0052	-0.00030	0.17
Bermuda	-0.0094	-0.011	-0.0094	-0.010	-0.0086	-0.0090	-0.0095	0.12
Kaashidhoo	-0.033	-0.031	-0.023	-0.025	-0.022	-0.018	-0.019	0.15
Midway Island	-0.00045	-0.0048	-0.0011	-0.0045	-0.0068	-0.0086	-0.0015	0.22
Ascension Island	-0.0077	-0.0090	-0.0071	-0.011	-0.011	-0.014	-0.0095	0.19
Tahiti	-0.012	-0.0042	-0.0040	-0.0065	-0.0029	-0.0041	-0.0029	0.050
Amsterdam Island	0.0068	-0.00042	-0.00097	-0.0037	-0.0042	-0.0099	-0.0068	0.20
Crozet Island	-0.0068	-0.0063	-0.0091	-0.0068	-0.0041	-0.012	-0.014	0.74
Guam	0.0064	0.0047	0.0029	-0.0029	-0.0016	-0.0056	-0.0026	0.15
Nauru	-0.0015	-0.0033	-0.0017	-0.0046	-0.0041	-0.0042	-0.0043	0.096
Graciosa	-0.021	-0.013	-0.012	-0.018	-0.013	-0.013	-0.016	0.18
				Scaled median absolute difference				
Lanai	0.011	0.0081	0.0057	0.0058	0.0061	0.0056	0.0061	0.13
Bermuda	0.021	0.021	0.018	0.018	0.016	0.015	0.014	0.19
Kaashidhoo	0.013	0.0094	0.0062	0.011	0.0068	0.0060	0.0056	0.19
Midway Island	0.014	0.013	0.010	0.0099	0.0084	0.0078	0.0078	0.10
Ascension Island	0.018	0.016	0.016	0.016	0.015	0.012	0.011	0.11
Tahiti	0.011	0.0074	0.0050	0.0053	0.0049	0.0046	0.0059	0.15
Amsterdam Island	0.011	0.0094	0.0080	0.0081	0.0091	0.0082	0.0054	0.10
Crozet Island	0.025	0.025	0.021	0.028	0.027	0.012	0.022	0.80
Guam	0.010	0.011	0.0087	0.0072	0.0059	0.0065	0.0079	0.12
Nauru	0.0086	0.0089	0.0071	0.0089	0.0049	0.0076	0.0074	0.13
Graciosa	0.017	0.014	0.013	0.011	0.0093	0.0093	0.0087	0.16

Table 11. Comparison between spectral AOD and α modelled using NCEP wind speed, and that measured on MAN cruises. The correlation coefficient is Pearson's linear correlation coefficient, and the bias is defined such that positive values mean the model is larger than the MAN data. The final column shows, for spectral AOD, the fraction of predicted AODs lying within the Sun-photometer typical uncertainty of ± 0.02.

Parameter	Number of matches	Correlation coefficient	Median bias	SMAD	Minimum MAN value	Maximum MAN value	Fraction within 0.02
τ_{440}	104	0.45	0.001	0.024	0.022	0.235	0.55
τ_{500}	135	0.43	0.006	0.021	0.021	0.175	0.62
τ_{675}	135	0.46	0.005	0.020	0.017	0.143	0.68
τ_{870}	135	0.54	0.0002	0.018	0.017	0.143	0.68
α	104	0.23	0.25	0.322	-0.053	1.16	-

Table 12. Lidar ratios S for unpolluted marine aerosol, calculated for 532 nm and 1064 nm. The top section presents results for bimodal lognormal distribution fits. The bottom section presents calculations for the exact averaged size distributions.

Distribution	Lidar ratio S	
	532 nm	1064 nm
Bimodal lognormal fits		
Recommended model	28.1	30.8
0-4 ms^{-1}	34.0	35.2
4-6 ms^{-1}	29.3	31.2
6-8 ms^{-1}	26.9	29.9
8-10 ms^{-1}	25.4	28.7
10+ ms^{-1}	25.0	30.7
Exact size distributions		
Lanai	30.3	33.3
0-4 ms^{-1}	35.9	35.9
4-6 ms^{-1}	31.3	33.6
6-8 ms^{-1}	29.3	33.0
8-10 ms^{-1}	28.2	32.3
10+ ms^{-1}	28.4	34.2

Table 13. Parameters for recommended aerosol model of unpolluted marine aerosol, for use in general satellite remote sensing applications.

Parameter	Value
	Fine mode
$r_{v,f}$	0.157 μm
σ_f	0.50
m	1.415 - 0.002i
	Coarse mode
$r_{v,c}$	2.58 μm
σ_c	0.72
m	1.363 - $3 \times 10^{-9}i$

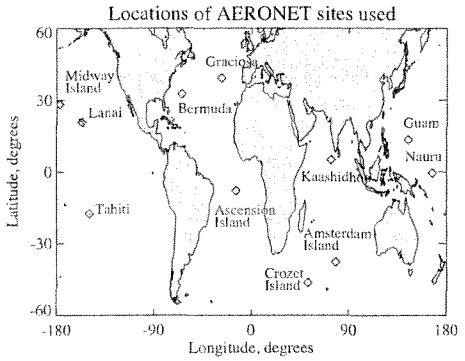

Figure 1. Locations of AERONET sites used in this work.

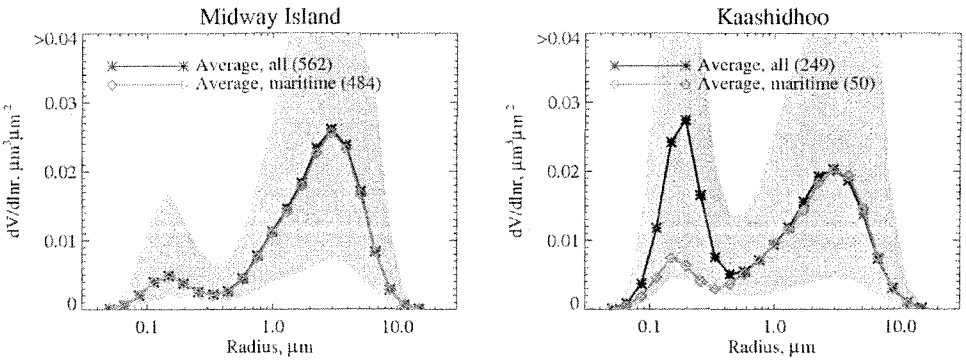

Figure 2. Averaged (median) retrieved aerosol volume size distributions at Midway Island (left) and Kaashidhoo (right), calculated from all retrieved size distributions (black), and only those distributions meeting the maritime criteria described in the text (red). The shaded region indicates the 5^{th} to 95^{th} percentiles of $dV(r)/d\ln(r)$ encountered in each size bin.

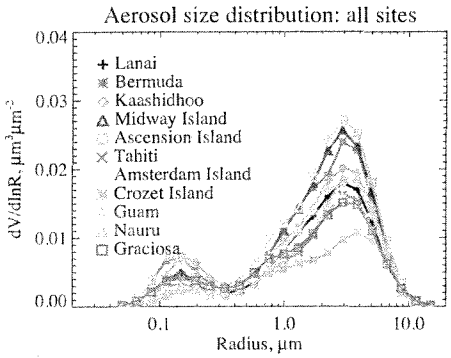

Figure 3. Averaged (median) aerosol volume size distributions for the AERONET sites in Table 1, for measurements corresponding to maritime-type size distributions as described in the text.

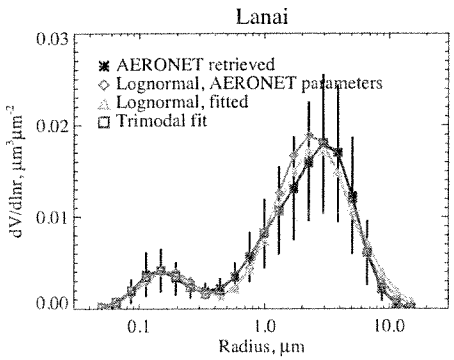

Figure 4. Averaged (median) retrieved aerosol volume size distributions for Lanai (black), and lognormal approximations to it. The distribution constructed from direct use of AERONET parameters is in red, the best-fit bimodal lognormal distribution is in green, and the best-fit trimodal lognormal distribution in blue. Error bars on the retrieved size distribution denote the scaled median absolute deviation, as described in the text.

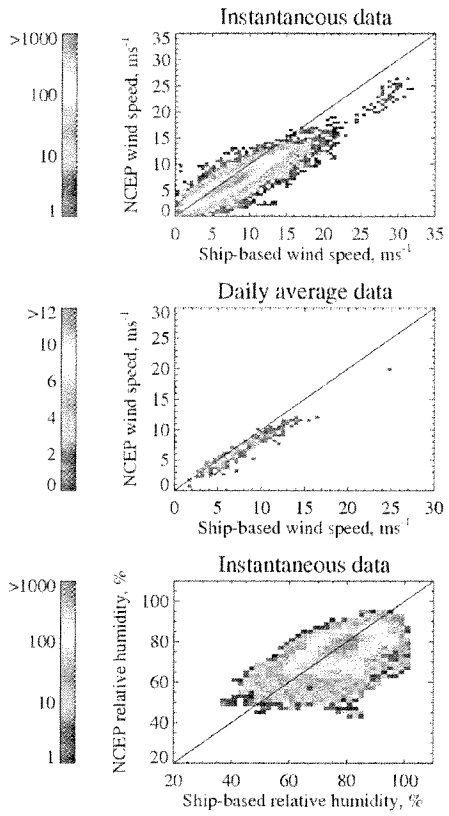

Figure 5. Scatter-density comparison between NCEP and ship-based measurements of wind speed and relative humidity. From top-bottom, plots show instantaneous wind speeds; daily-averaged wind-speeds; and instantaneous relative humidity. Bins without data are shown in white. The bin size is 0.5 ms^{-1} for wind speed and 2 % for relative humidity. The 1:1 line is overplotted.

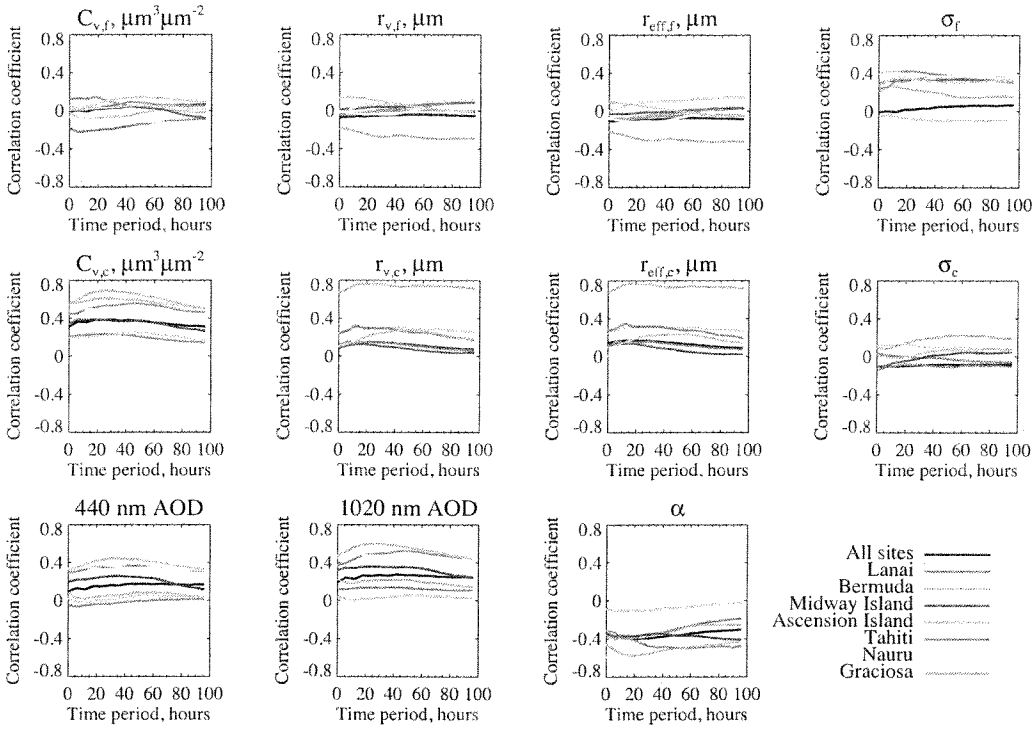

Figure 6. Pearson's linear correlation coefficient between time-averaged wind speed and AERONET aerosol properties, for all data combined (black lines) and those sites with 100 or more AERONET retrievals (coloured lines). Data for the AERONET aerosol size distribution product (*Dubovik and King*, 2000).

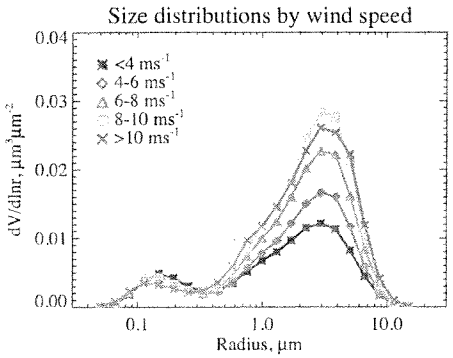

Figure 7. Averaged (median) AERONET aerosol volume size distributions, binned by near-surface wind speed.

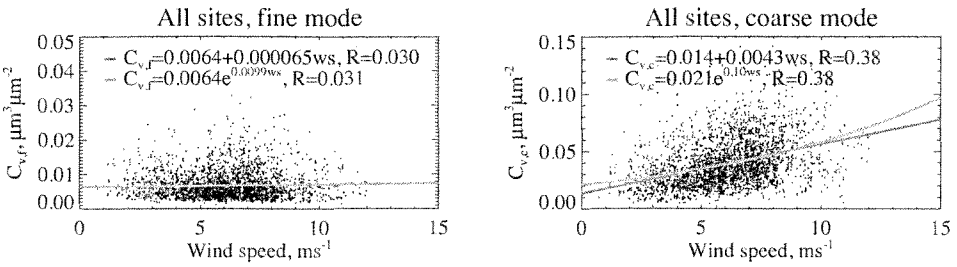

Figure 8. Linear (red) and exponential (green) regression fits of aerosol volume to 24-hour-averaged wind speed for fine (left) and coarse (right) mode data from all AERONET sites considered together. Regression statistics are given in the plots. R is Pearson's linear correlation coefficient for the fit.

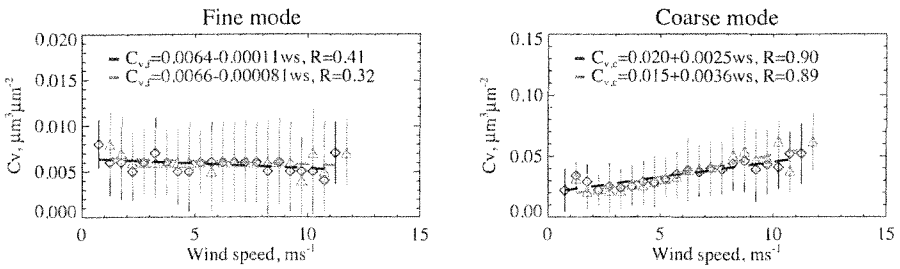

Figure 9. Relationship between wind speed and aerosol volume for fine (left) and coarse (right) modes, binned by wind speed in bins of 0.5 ms^{-1}. Black diamonds show data binned by spatio-temporally interpolated NCEP wind speeds, and red triangles data binned by NCEP wind speed averaged over the 24-hour-period prior to the retrieval. Error bars show the standard deviation on each bin's data. Coefficients of linear fit are given in the plots, and illustrated with dashed lines; R indicates Pearson's linear correlation coefficient. Data are only shown where a bin contains at least 10 data points.

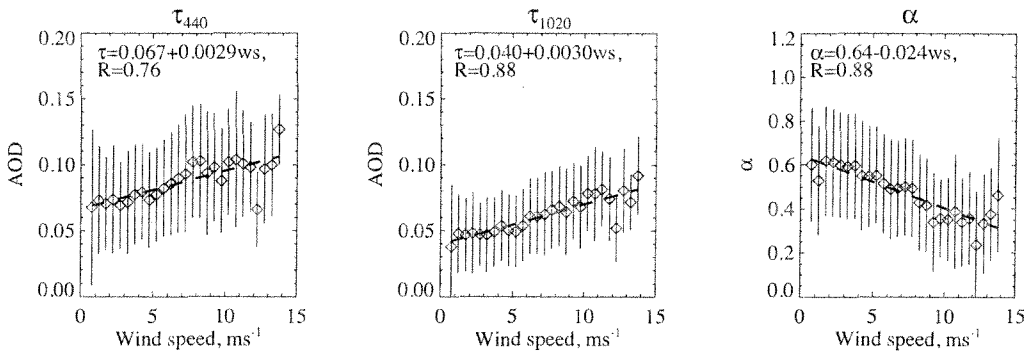

Figure 10. Relationship between daily averages of wind speed and AOD at 440 nm (left), AOD at 1020 nm (middle), and α (right), binned by wind speed in bins of 0.5 ms^{-1}. Bin medians are used, and error bars show the standard deviation on each bin's data. Coefficients of linear fit are given in the plots, and illustrated with dashed lines; R indicates Pearson's linear correlation coefficient. Data are only shown where a bin contains at least 10 data points.

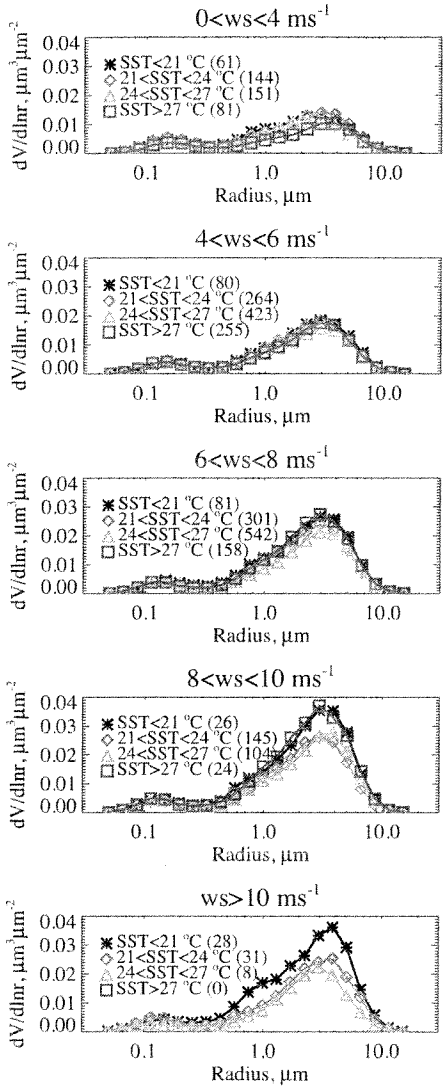

Figure 11. Averaged (median) AERONET aerosol volume size distributions, arranged by near-surface 24-hour-averaged wind speed (top to bottom, range indicated above plots), and binned according to the 24-hour-averaged SST. The number of size distribution inversions contributing to each line is given in the legend.

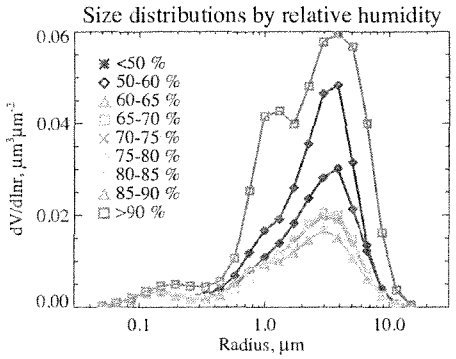

Figure 12. As Figure 7, except binned by relative humidity.

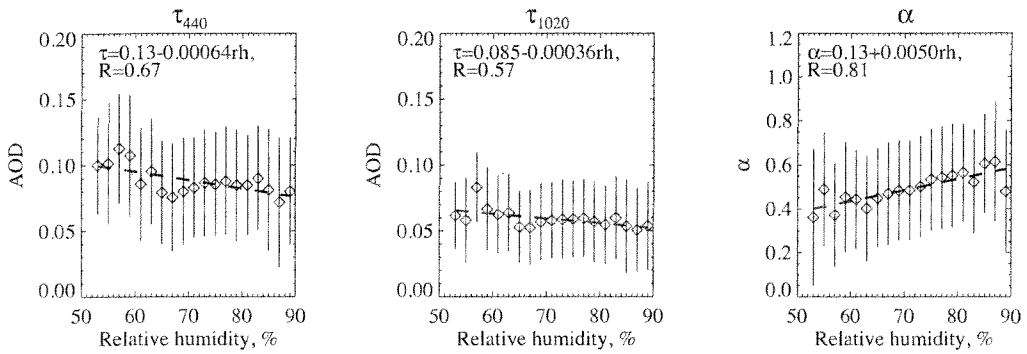

Figure 13. Relationship between daily averages of relative humidity and AOD at 440 nm (left), AOD at 1020 nm (middle), and α (right), binned by relative humidity in bins of 2 %. Bin medians are used, and error bars show the standard deviation on each bin's data. Coefficients of linear fit are given in the plots, and illustrated with dashed lines; R indicates Pearson's linear correlation coefficient. Data are only shown where a bin contains at least 10 data points.

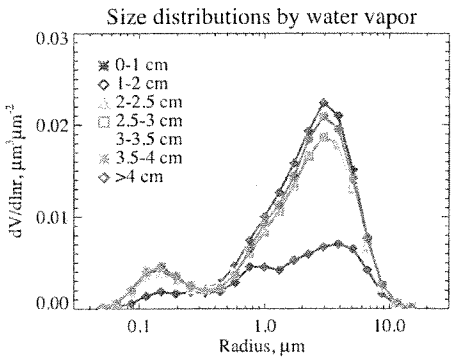

Figure 14. As Figure 7, except binned by AERONET columnar water vapor amount.

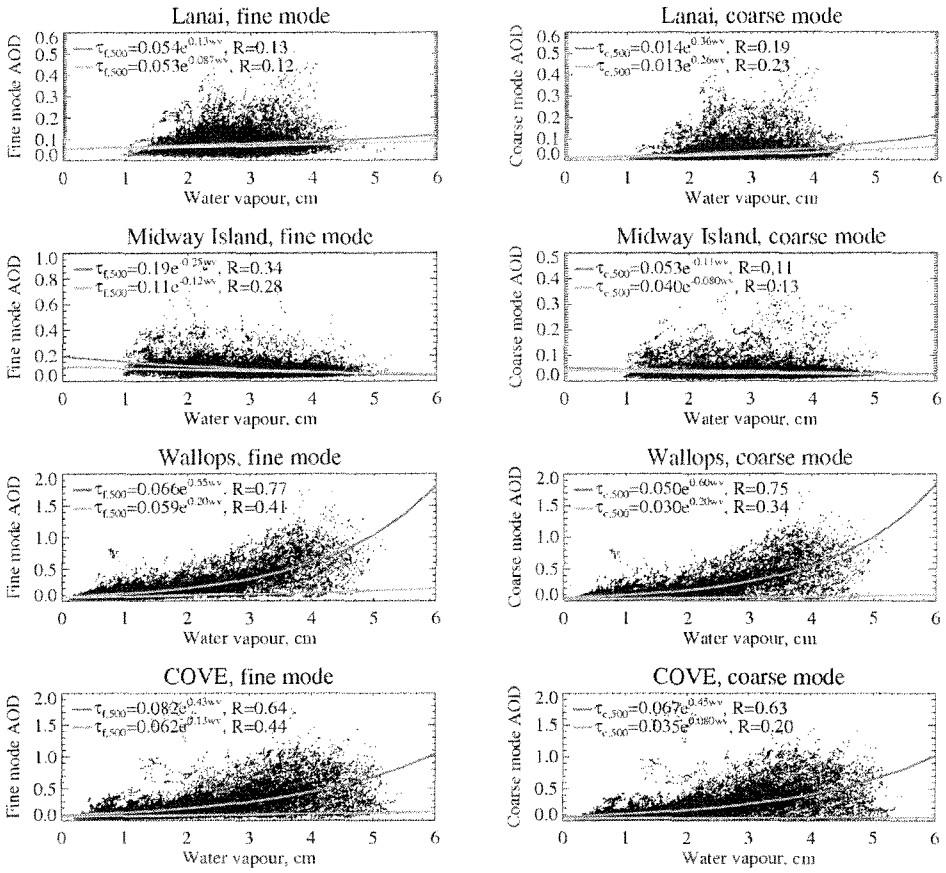

Figure 15. Relationship between water vapor content (wv) and $\tau_{f,500}$ (left) or $\tau_{c,500}$ (right) from the AERONET SDA product, for four sites. In each case, the red line indicates an exponential fit to all points, and the green line an exponential fit to only those points where $\tau_{500} \leq 0.2$ and $0.1 \leq \alpha \leq 1$ (deemed maritime conditions). The equation of each fit line, and Pearson's linear correlation coefficient of the fit (R), are given in each plot.

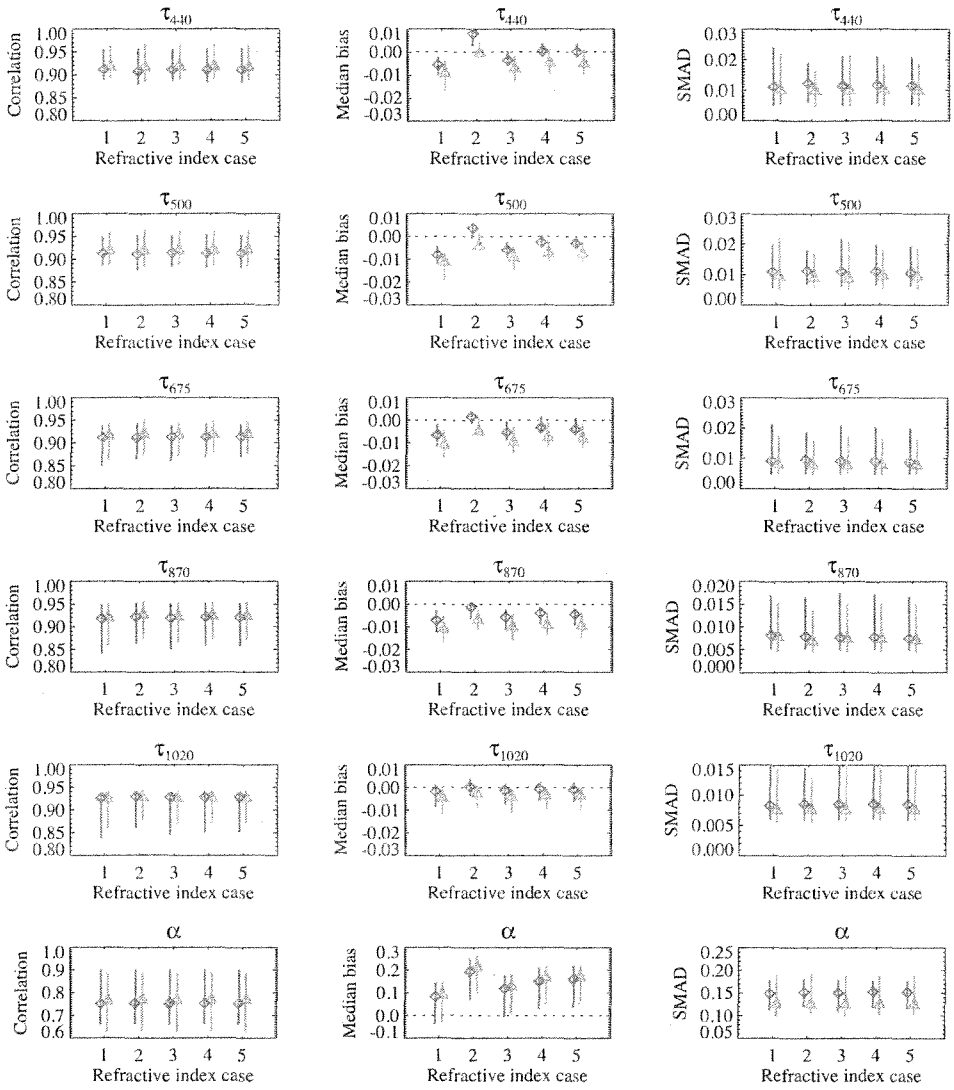

Figure 16. Statistics of comparison of spectral AOD and Ångström exponent between AERONET retrievals, and calculations performed using the average aerosol size distribution parameters, for a variety of assumed aerosol refractive indices (cases in Table 9). Subfigures show Pearson's linear correlation coefficient (left), median bias (centre), and SMAD (right). Red diamonds indicate the 'AERONET lognormal' approach and green triangles the 'lognormal fitted' method, slightly offset along the x-axis for clarity. Symbols show the median, and error bars the minimum and maximum values, over the ensemble of five sites used for the evaluation.

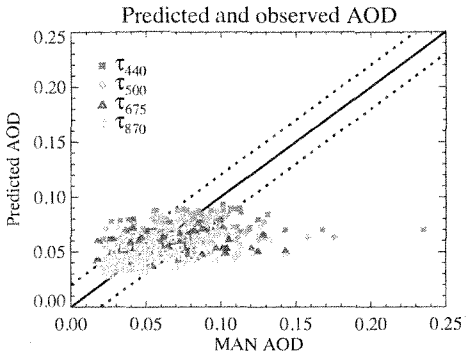

Figure 17. Comparison between MAN AODs and those predicted using the wind-speed relationship from AERONET sites. The solid line is the 1:1 line, and the dotted lines indicate the MAN uncertainty of ± 0.02.